Solute-strengthening in metal alloys with short-range order

S. Nag[a,b], W. A. Curtin[a]

[a]*Institute of Mechanical Engineering, École Polytechnique Fédérale de Lausanne, EPFL STI IGM Station 9, CH-1015 Lausanne*
[b]*Currently at Materials Modeling Division, Technical University of Darmstadt, Otto-Berndt-Str. 3, 64206 Darmstadt*

Abstract

Recent surging interest in strengthening of High Entropy Alloys (HEAs) with possible chemical ordering motivates the development of new theory. Here, an existing theory for random alloys that accounts for solute-dislocation and solute-solute interactions is extended to include strengthening due to short-range order (SRO). Closed form expressions are presented for the yield strength and energy barrier of dislocation motion in alloys with SRO based on inputs of atomic misfit volumes, average lattice and elastic constants, the SRO parameters, and effective pair interactions between solutes. The theory shows both the long-established athermal strengthening effect of SRO as well as a notable effect of SRO on the misfit volume strengthening, which can increase or decrease strength. The generalized solute-strengthening theory is the most comprehensive to date that is applicable to macroscopically homogeneous single-phase alloys using inputs that can be measured, computed, or estimated.

Keywords: short-range order, Warren-Cowley SRO parameter, yield strength, average-strengthening

1. Introduction

Scientific and technological interest in both dilute solute-strengthened alloys (Al-Mg, Mg-Y, Ni-Al, and many others) and high-entropy alloys (HEAs), which are essentially high-concentration solute-strengthened materials, has led to the development of a general theoretical model [1–5] to predict solute strengthening in random alloys. The theory is based on solute/dislocation interaction energies and shows that strengthening arises because dislocations become wavy to find local favorable fluctuations in the solute arrangements, and the dislocations are pinned in these local environments. A combination of stress and thermal activation is then required for dislocation motion and associated temperature- and strain-rate-dependent plastic flow. The strengthening theory was recently extended to include the effects of specific solute-solute interactions in random alloys [6].

Solute-solute interactions also drive the formation of short-range order (SRO) and long-range order (LRO) (phase separation or precipitation). SRO arises due to a combination of the thermodynamic driving forces of solute-solute interactions and the kinetics of solute transport. With decreasing temperature, the thermodynamic driving force increases but solute diffusion decreases. Thus, SRO usually arises in intermediate temperature domains in between the high-T domain of an essentially random solution and a low-T kinetically-inhibited domain where equilibrium SRO or LRO cannot be achieved. Operationally, many alloys are heat-treated or annealed at some temperature T_a and then quenched to low T. For very rapid quenching, the SRO in the alloy is then determined mainly by T_a. However, for slower cooling, further SRO may form during the time spent at lower temperatures until temperatures are reached at which kinetics inhibits further SRO. Thus, while SRO is well-defined thermodynamically at any temperature, the degree of SRO actually arising in real materials is unclear and dependent on processing.

SRO was extensively studied experimentally and theoretically in binary alloys in the 1950s and 1960s [7–11]. New analytical tools and the emergence of first-principles calculations have both enabled more detailed characterization of SRO in binary alloys [12–14] and its possible influences on strength and stacking fault energy [15–17]. Recent emphasis on HEAs has further driven efforts to determine if SRO exists in these alloys and, if it exists, its effects on alloy properties such as strength [18–27]. To date, there is no full theory for alloy strengthening in the presence of SRO. The early theories for strength due to SRO predict zero strength in the absence of SRO, and so are incomplete.

*Shankha Nag (shankha.nag@epfl.ch)

In this paper, we derive a general theory for solute-strengthening including SRO. In the limit of no SRO (random alloys), the theory reverts to the recent theory of Nag et al. [6]. SRO creates two main sources of additional strengthening, for which we derive analytical expressions. The first strengthening effect is due to dislocation slip that destroys/reduces SRO. Since SRO is an energetically favorable distribution of the different constituent species in the alloy, the destruction of SRO by dislocation slip requires additional energy and hence additional applied stress to drive the dislocation. This creates a temperature-independent athermal strengthening that was first addressed qualitatively by Fisher [9]. Existing theories of this strength contribution [10, 11, 23] exist for special/limiting cases; here we derive results for arbitrary alloys and then present limiting cases to make contact with earlier results. The second strengthening effect is due to changes in the local solute fluctuations in the presence of SRO, which affects the collective solute/dislocation interaction energies. The effect of SRO on solute/dislocation interactions caused by solute misfit volumes exists even if the direct solute-solute interactions (which actually cause the SRO) are neglected. A main *derived* result is that this effect of SRO can *decrease* alloy strength under some circumstances, providing a rigorous basis for a recent claim of this effect in Ref. [23].

To predict the role of SRO on alloy strength, SRO must be clearly defined. This is done in Section 2 in terms of multi-solute correlation functions, leading to the well-known Warren-Cowley SRO parameters for pair correlations [7, 28, 29]. Section 3 introduces solute-solute interactions in terms of Effective Pair Interactions (EPIs) which control chemical ordering and also influence alloy strength in the presence of SRO. Section 4 then presents the theory for strengthening in the presence of SRO. Subsection 4.1 derives the results for the athermal average strengthening while Subsection 4.2 derives the strengthening contributions due to fluctuations. Section 5 furthers simplifies the strengthening theory using a linear elasticity approximation for the solute/dislocation interaction energies, which leads to analytic results and enables insights into the effects of SRO. Section 6 summarizes the main outcomes of the present work.

2. Characterizing short-range order

Short-range order (SRO) is a spatially homogeneous state of an alloy. Local clustering of atoms, which may occur prior to phase segregation or spinodal decomposition is *not* SRO. Here, we review the definition of SRO in a multicomponent alloy.

In a spatially homogeneous alloy of N elemental components at compositions c_n, the probability of a site i being occupied by an atom of type n is c_n. However, unlike random alloys, alloys with short-range order (SRO) have correlated site occupations. That is, the joint probability of occupation of sites i and j by atoms of type n and m is not simply the product $c_n c_m$ for all site pairs (i, j). To proceed formally, we first define a site occupation variable s_i^n as

$$s_i^n = \begin{cases} 1 & \text{if site } i \text{ has atom type } n \\ 0 & \text{otherwise} \end{cases} \tag{1}$$

$$\tag{2}$$

where, for all sites i,

$$\sum_n s_i^n = 1 \quad \text{and} \quad s_i^n s_i^m = 0, \quad n \neq m \tag{3}$$

$$\tag{4}$$

with the latter indicating that any given site can only have one solute.

Next we define $\mathbf{P}(s_i^n = 1, s_j^m = 1, \dots)$ as the probability of an alloy configuration where distinct atomic sites $i, j, \dots$ are occupied by solute types $n, m, \dots$ respectively. We can then define the multisite correlation

functions $\lambda^{ij\ldots}_{nm\ldots}$ for distinct sites $i, j, k, \ldots$ as

$$\mathbf{P}(s_i^n = 1) = \sum_{m,p,\ldots} \mathbf{P}(s_i^n = 1, s_j^m = 1, s_k^p = 1, s_l^q = 1, s_u^t = 1, \ldots) = c_n, \tag{5a}$$

$$\mathbf{P}(s_i^n = 1, s_j^m = 1) = \sum_{p,q,t,\ldots} \mathbf{P}(s_i^n = 1, s_j^m = 1, s_k^p = 1, s_l^q = 1, s_u^t = 1, \ldots) = \lambda^{ij}_{nm}\, c_n c_m, \tag{5b}$$

$$\mathbf{P}(s_i^n = 1, s_j^m = 1, s_k^p = 1) = \sum_{q,t,\ldots} \mathbf{P}(s_i^n = 1, s_j^m = 1, s_k^p = 1, s_l^q = 1, s_u^t = 1, \ldots) = \lambda^{ijk}_{nmp}\, c_n c_m c_p, \tag{5c}$$

$$\mathbf{P}(s_i^n = 1, s_j^m = 1, s_k^p = 1, s_l^q = 1) = \sum_{t,\ldots} \mathbf{P}(s_i^n = 1, s_j^m = 1, s_k^p = 1, s_l^q = 1, s_u^t = 1, \ldots) = \lambda^{ijkl}_{nmpq}\, c_n c_m c_p c_q, \tag{5d}$$

$\vdots$

where $\lambda^{ij}_{nm}, \lambda^{ijk}_{nmp}, \lambda^{ijkl}_{nmpt}$ are pair, 3-site, 4-site correlation functions. *Henceforth, different site indices will mean different physical sites unless in summations or specifically noted otherwise. Also repeated indices will NOT imply Einstein summation in this article.* In random alloys, all site occupancies are independent and so all the correlation functions are equal to 1. Spatial homogeneity dictates that the correlation functions be invariant under various symmetry operations such as translation, rotation, reflection, etc. This means, for example, that $\lambda^{ij}_{nm} = \lambda^{ij}_{mn}$.

Since the correlation functions are normalized probabilities, they obey certain identities and inequalities that follow from probability theory [30]. For example, the conditional probability $\mathbf{P}(s_i^n = 1 \big| s_j^m = 1)$ of finding a type n atom at site i *given* that site j is occupied by a type m atom can be written as

$$\mathbf{P}(s_i^n = 1 \big| s_j^m = 1) = \lambda^{ij}_{nm}\, c_n$$
$$\mathbf{P}(s_i^m = 1 \big| s_j^n = 1) = \lambda^{ij}_{mn}\, c_m$$

Using $\lambda^{ij}_{nm} = \lambda^{ij}_{mn}$ and noting that the probability must be in the range $[0, 1]$ leads to the restrictions

$$0 \le \lambda^{ij}_{nm} \le \min\left(\frac{1}{c_n}, \frac{1}{c_m}\right) \tag{6}$$

The pair correlation functions are also not independent. Since the sum of all pair probabilities equals 1, we have

$$\sum_n \mathbf{P}(s_i^n = 1 \big| s_j^m = 1) = 1 \implies \sum_n \lambda^{ij}_{nm}\, c_n = 1 \quad \forall m \tag{7}$$

The pair correlation functions for solutes of the same type thus can be expressed in terms of the pair correlation functions of solutes of unlike types as

$$\lambda^{ij}_{mm} = \frac{1}{c_m}\left(1 - \sum_{\substack{n \\ n \neq m}} \lambda^{ij}_{nm} c_n\right) \quad \forall m \tag{8}$$

Finally, the pair correlations for alloys with SRO are widely characterized by the Warren-Cowley parameters α^{ij}_{nm} [7] defined as

$$\alpha^{ij}_{nm} = 1 - \frac{\mathbf{P}(s_i^n = 1 \big| s_j^m = 1)}{c_n}. \tag{9}$$

Using Equation 5b, we find

$$\alpha^{ij}_{nm} = 1 - \frac{\mathbf{P}(s_i^n = 1, s_j^m = 1)}{c_n c_m} = 1 - \lambda^{ij}_{nm} \tag{10}$$

In our analysis below, we will mainly use λ rather than α for convenience, and convert to the use of α only in final results. Equations 8 can be rewritten in terms of the Warren-Cowley parameters as

$$\alpha^{ij}_{mm} = -\frac{1}{c_m} \sum_{\substack{n \\ n \neq m}} \alpha^{ij}_{nm} c_n \quad \forall m. \tag{11}$$

This important sum-rule is often overlooked in the literature, but is useful in reducing analytical results to clearly-interpretable forms, as we will see below.

The WC SRO parameters are approximately (*but not exactly, due to multisite correlations*) related to the underlying solute-solute interactions as

$$\alpha_{nm}^{ij}\begin{cases} >0 & \text{solute-pairs } n-m \text{ at sites } i,j \text{ tend to repel} \\ =1 & \text{solute-pairs } n-m \text{ at sites } i,j \text{ tend to not interact} \\ <0 & \text{solute-pairs } n-m \text{ at sites } i,j \text{ tend to attract} \end{cases} \tag{12}$$

If solute interactions are large, then this drives phase formation/segregation. So, the WC-SRO parameters are often small ($\sim \pm 0.2$) in reasonably-concentrated alloys over a range of solute interaction energies, as observed in recent Monte-Carlo simulations [31].

With all of the above definitions of SRO clarified, we assess below how the presence of SRO ($\alpha_{ij}, \alpha_{ijk}, \ldots \neq 0$) affects alloy strengthening.

3. Solute-solute interactions

We first discuss the solute-solute interactions that create SRO. The total energy of an alloy can be formally decomposed into multi-body contributions using a cluster expansion. The cluster expansion (CE) involves a hierarchy of pair, triplet, etc. solute-solute interactions at different pair distances, triplet inner angle, etc. in a given lattice structure [32–34]. Once a CE is determined by fitting to a set of first-principles reference energies, SRO can then be modeling using the CE Hamiltonian and Monte Carlo simulations [35, 36]. For accurate thermodynamic predictions, which is the usual domain of application of the CE method, very high accuracy in the total energy versus atomic configuration is needed. However, for understanding solute strengthening contributions from the same solute-solute interactions, the same level of accuracy is not needed. At the same time, formulating a theory of solute strengthening in the presence of multibody (beyond pair) solute-solute interactions is daunting. Here, we thus model the total energy of an alloy in terms of pair energies at various lattice distances.

There are several possible formulations for the relevant solute-solute pair interactions. The simplest characterization is a description of the system energy in terms of pair potentials $U_{pq}(d)$ between solute types p and q at all the distances d in the crystal. The potential energy of the alloy for a given atom configuration (characterized by site occupation variables $\{s_i^p\}$) is given by

$$U = \frac{1}{2}\sum_{\substack{i,j \\ i\neq j}}\sum_{p,q} s_i^p s_j^q U_{pq}(d_{ij}) \tag{13}$$

where we are summing pair energies of unlike site pairs $\{i,j\}$. However, since only changes in energy are relevant to both SRO and solute strengthening, the expression for total potential energy U can be rearranged as

$$\begin{aligned} U &= -\frac{1}{4}\sum_{\substack{i,j \\ i\neq j}}\sum_{p,q} s_i^p s_j^q V_{pq}^{eff}(d_{ij}) + \frac{1}{2}\sum_i\sum_p s_i^p \sum_{\substack{j \\ j\neq i}} U_{pp}(d_{ij}) \\ &= -\frac{1}{4}\sum_{\substack{i,j \\ i\neq j}}\sum_{p,q} s_i^p s_j^q V_{pq}^{eff}(d_{ij}) + \frac{1}{2}\sum_i\sum_p s_i^p \varepsilon_i^p \end{aligned} \tag{14}$$

where the effective pair interaction (EPI) $V_{pq}^{eff}(d_{ij})$ between atoms p and q at distance d_{ij} is given by

$$V_{pq}^{eff}(d_{ij}) = U_{pp}(d_{ij}) + U_{qq}(d_{ij}) - 2U_{pq}(d_{ij}) \tag{15}$$

Equation 14 also involves single-site energies

$$\varepsilon_i^p = \sum_{\substack{j \\ j\neq i}} U_{pp}(d_{ij}) \tag{16}$$

In a perfect crystal, this single-site energy is independent of i and so is just a configuration-independent constant energy. However, for a crystal containing a stacking fault, where the local atomic structure differs

from the perfect crystal, the single-site energy will enter into the analysis. Note that the EPIs for like-atom pairs are zero, so there are only $N(N-1)/2$ independent EPIs at each distance in an N-component alloy, i.e. the same as the number of independent WC SRO parameters.

Equation 14 is a cluster expansion derived from pair interatomic potentials. However, the EPIs and site energies can be obtained by fitting the cluster expansion of Equation 14 to any set of alloy reference energies obtained by many-body interatomic potentials or first principles at the desired composition [6, 37].

Given a set of EPIs versus interatomic distance, SRO can be computed using Monte Carlo methods. Describing the system energy with EPIs does not eliminate the possibility of higher order correlations. In addition, the resulting SRO depends on the accuracy of the EPIs as compared to more detailed cluster expansions. For given EPIs, the SRO parameters can also be estimated analytically [31] for high temperatures or small EPIs, where the SRO is moderate.

4. Solute-strengthening in alloys with SRO

In a random or SRO alloy, an initially straight dislocation segment becomes spontaneously wavy to lower its total energy. Local dislocation segments glide into regions of the alloy where the local arrangement of solutes interacts favorably (lower energy) with the dislocation. This lowering of the energy due to interactions with solute fluctuations is offset by the increased line or elastic energy of the wavy dislocation relative to the straight dislocation. Together, these energetic features establish a characteristic waviness with wavelength $4\zeta_c$ and amplitude w_c. Segments of length ζ_c then lie in local energy minima, and a combination of stress and temperature is required to enable thermal activation of these segments over their adjacent unfavorable high-energy environments at a typical glide distance w_c. The goal of solute-strengthening theory is then to compute the characteristic scales (ζ_c, w_c), the associated energy barrier ΔE_b, and zero-temperature flow stress τ_{y0}. The full temperature- and strain-rate-dependent yield stress $\tau_y(\dot{\varepsilon}, T)$ can then be determined using standard thermal activation theory.

In the presence of SRO, the shearing of the alloy due to dislocation glide destroys the SRO across the glide plane. This loss of SRO increases the total energy of the system, and so is an energy cost γ_{SRO} per unit area of glide that must be overcome by the work done by the applied stress. The strengthening of an alloy with SRO thus has two components, as indicated in Figure 1: the strengthening due to loss of SRO over the glide plane (*athermal strengthening*) and the strengthening due to the local waviness caused by the fluctuations in the solute configuration along the dislocation line (*local strengthening*).

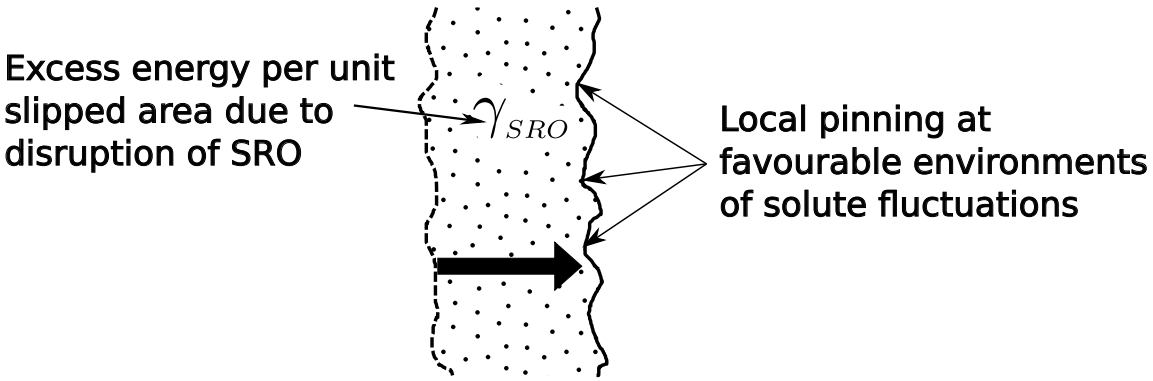

Figure 1: Schematic representation of "average" and "local" strengthening in alloys. Average strengthening is related to the stress required to pay the energy penalty associated with the disruption of SRO due to dislocation glide, denoted as γ_{SRO} in the figure. Local strengthening due to fluctuations is related to the stress required to unpin dislocation segments in a wavy configuration where dislocation segments move into local favourable solute environments.

The solute-strengthening analysis begins with an analysis of the total energy change $\Delta E_{\mathrm{p}}(\zeta, w)$ of a dislocation line of length ζ as it glides through the alloy over a distance w. There are two contributions to the energy change. The first is due to the solute-dislocation interaction energy $U^n_{sd}(x,y)$ between a type n solute at position (x,y,z) relative to a straight dislocation at $x=0, y=0$ parallel to the z-axis (with x the glide direction and y the slip plane normal). A gliding dislocation line sees different solute environments relative to its position, and hence a fluctuating potential energy. The individual solute-dislocation interactions are assumed to be independent of any SRO. For a specific configuration of atoms defined by the occupation

variables $\{s_i^n\}$, the potential energy change ΔE_{sd} of a segment of length ζ due to glide of distance w is then

$$\Delta E_{sd} = \sum_i \sum_n s_i^n \left(U_{sd}^n(x_i - w, y_i) - U_{sd}^n(x_i, y_i) \right) \tag{17}$$

where i runs over all lattice positions within a slice of alloy of width ζ along the dislocation line direction and n runs over all solute types of the alloy. We suppress the dependence of ΔE_{sd} on ζ and w for simplicity.

The second contribution to the energy change is due to solute-solute interactions, arising from the change in solute environments across the slip plane in the slipped area swept by the dislocation line while gliding by distance w. This contribution is labelled as ΔE_{ss} where again ζ and w dependencies are suppressed. We discuss the calculation of ΔE_{ss} below, but here we first discuss its inclusion into the general theory. The role of ΔE_{ss} depends on crystal structure, differing between bcc (with a compact core) and fcc (with a dissociated or split core) systems (see [6]). For a dislocation with compact core, a segment of length ζ gliding by distance w leaves behind a fully slipped area of size ζw (see Figure 2). The associated energy change in this case is denoted as $\Delta E_{ss,f}$ where the subscript f indicates full slip. For a dissociated dislocation with partial separation distance d_p, as in fcc crystals, two cases arise depending on the gliding distance w relative to d_p (see Figure 2). If $w < d_p$, a gliding segment repairs a stacking fault of area ζw behind the trailing partial and creates a new stacking fault of area ζw behind the leading partial. We denote these energy changes by $\Delta E_{ss,p-}$ and $\Delta E_{ss,p+}$ respectively with the subscript p indicating partial slip. The total energy change due to solute-solute interaction is then $\Delta E_{ss} = \Delta E_{ss,p-} + \Delta E_{ss,p+}$. On the other hand, if $w > d_p$ then the gliding segment repairs a stacking fault of area ζd_p behind the trailing partial and creates a new stacking fault of area ζd_p behind the leading partial and also leaves behind a fully slipped region of area $\zeta(w - d_p)$. The total energy change due to solute-solute interactions is then $\Delta E_{ss} = \Delta E_{ss,p-} + \Delta E_{ss,p+} + \Delta E_{ss,f}$.

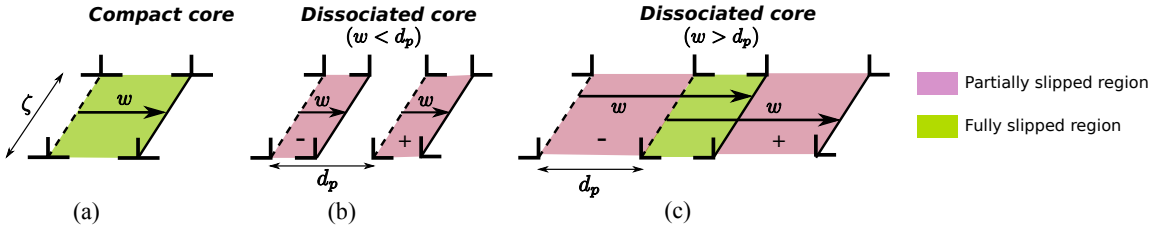

Figure 2: Schematic of areas swept during dislocation glide by a distance w. (a) bcc crystal (no dissociation); (b) fcc crystal (dissociated core) with $w < d_p$; (c) fcc crystal (dissociated core) with $w > d_p$. The + and - sign on the stacking faults signifies the lost and newly formed fault areas as a result of dislocation glide. (Reproduced from Ref. [6])

Each of the energy contributions $\Delta E_{ss,p-}$, $\Delta E_{ss,p+}$ and $\Delta E_{ss,f}$ can be directly calculated using atomistic simulations or first-principles. Here, we express them in terms of the effective pair interactions V_{pq}^{eff}(s) and site energies ε_i^p (see Equation 14) as

$$\Delta E_{ss,f} = -\frac{1}{2} \sum_{k,l} \sum_{p,q} s_k^p s_l^q \left(V_{pq}^{eff}(d_{kl}^f) - V_{pq}^{eff}(d_{kl}) \right); \quad d_{kl}^f = ||\boldsymbol{r}_{kl} + \boldsymbol{b}|| \tag{18a}$$

$$\Delta E_{ss,p+} = -\frac{1}{2} \sum_{k,l} \sum_{p,q} s_k^p s_l^q \left(V_{pq}^{eff}(d_{kl}^p) - V_{pq}^{eff}(d_{kl}) \right) + \frac{1}{2} \sum_i \sum_p s_i^p \Delta\varepsilon_i^p; \quad d_{kl}^p = ||\boldsymbol{r}_{kl} + \boldsymbol{b}_p|| \tag{18b}$$

$$\Delta E_{ss,p-} = \frac{1}{2} \sum_{k,l} \sum_{p,q} s_k^p s_l^q \left(V_{pq}^{eff}(d_{kl}^p) - V_{pq}^{eff}(d_{kl}) \right) - \frac{1}{2} \sum_i \sum_p s_i^p \Delta\varepsilon_i^p; \quad d_{kl}^p = ||\boldsymbol{r}_{kl} + \boldsymbol{b}_p|| \tag{18c}$$

where sites k are below the slip plane and sites l are above the slip plane, because any pair of sites on the same side of the slip plane is unaffected by the slip. The sum over i is over all sites, $\boldsymbol{b}$ and $\boldsymbol{b}_p$ are the full and partial Burgers vectors respectively, and $\boldsymbol{r}_{kl}$ is the vector from site k to site l. Finally, $\Delta\varepsilon_i^p$ is the change in site energy ε_i^p of atom type p at site i after partial slip by b_p due to the change in atomic coordination around site i. In Equation 18 we have ignored the dislocation displacement field which deviates negligibly from the displacement jump ($\boldsymbol{b}$ and $\boldsymbol{b_p}$) near the glide plane away from the dislocation core.

The total potential energy change of a segment of length ζ after glide by a distance w is thus

$$\Delta E_{\mathrm{p}}(\zeta, w) = \Delta E_{sd}(\zeta, w) + \Delta E_{ss}(\zeta, w) \tag{19}$$

where we have now made the ζ and w dependencies explicit for clarity. Strengthening, as derived later below, will depend on both the average energy change $\langle \Delta E_{\mathrm{p}} \rangle$ averaged over all possible configurations of solutes consistent with the SRO and the standard deviation (fluctuations) $\sigma_{\Delta E_{\mathrm{p}}}$ in energy.

4.1. Athermal strengthening due to SRO

In alloys with SRO, slip by a full Burgers vector over a large area A_{slip} is associated with an average energy penalty $\langle \Delta E_{\rm p} \rangle > 0$ since the favourable SRO state is disrupted for atom pairs across across the slip plane. This energy cost must be provided by an additional applied stress, independent of temperature, and hence this additional applied stress constitutes an athermal strengthening τ_A. Specifically, the work $\tau_A b A_{slip}$ by the stress τ_A acting over A_{slip} must equal the energy cost $\langle \Delta E_{\rm p} \rangle$. Hence, with $\Delta E_{\rm p} \propto A_{slip}$, the athermal strengthening is

$$\tau_A = \frac{1}{b} \frac{\langle \Delta E_{\rm p} \rangle}{A_{slip}} = \gamma_{SRO}/b \tag{20}$$

where γ_{SRO} the excess energy per unit area of slip, analogous to an antiphase boundary in the shearing of ordered phases.

$\langle \Delta E_{\rm p} \rangle$ has two contributions: $\langle \Delta E_{sd} \rangle$ due to changes in solute-dislocation interactions and $\langle \Delta E_{ss,f} \rangle$ due to changes in solute-solute interactions associated with full slip. However, since $< s_i^n >= c_n$ and $U_{sd}^n(x_i - w, y_i) - U_{sd}^n(x_i, y_i)$ summed over all sites i is zero, there is no average/non-fluctuating contribution from solute-dislocation interactions, which is not surprising. The contribution $\langle \Delta E_{ss,f} \rangle$ involves the average $\langle s_k^p s_l^q \rangle = \lambda_{pq}^{kl} c_p c_q$ (see equation 5) and so

$$\langle \Delta E_{ss,f} \rangle = -\frac{1}{2} \sum_{p,q} c_p c_q \sum_{k,l} \lambda_{pq}^{kl} \left(V_{pq}^{eff}(d_{kl}^f) - V_{pq}^{eff}(d_{kl}) \right) \tag{21}$$

After full slip by b, the crystal structure and hence atom pair distances remain unchanged so that the pair distances d_{kl} before and d_{kl}^f after slip belong to the same set of pair distances. For fcc, we have $d_{kl}/a \in \{1/\sqrt{2}, 1, \sqrt{3/2}, \sqrt{2}, \dots\}$ and for bcc we have $d_{kl}/a \in \{\sqrt{3}/2, 1, \sqrt{2}, \sqrt{11}/2, \dots\}$. To render Equation 21 useful, we define the quantities $n_{dd'}$, N_d and M_d (where indices $d, d' \in \{d_{kl}\}$) as

1. $n_{dd'}$ the number of pairs across the slip plane (per lattice site on the slip plane) at pair distance d before slip and at pair distance d' after slip for $d \neq d'$, and set convention $n_{dd'} = 0$ for $d = d'$;
2. N_d the number of pairs across the slip plane (per lattice site on the slip plane) at pair distances $\neq d$ before slip and at pair distance d after slip, so $N_d = \sum_{d'} n_{d'd}$;
3. M_d the number of pairs across the slip plane (per lattice site on the slip plane) at pair distance d before slip and at any pair separation $d' \neq d$ after slip, so $M_d = \sum_{d'} n_{dd'}$.

Table 1 tabulates $n_{dd'}$ for pair distance (d, d') up to 10 nearest-neighbor distances for full slip in fcc and bcc. Note that structure factors $\Theta_{dd'}$ in Ref. [6] are related to N_d, M_d and $n_{dd'}$ as $\Theta_{dd'} = (N_d + M_d)\delta_{dd'} - (n_{d'd} + n_{dd'})(1 - \delta_{dd'})$.

	d'/a \ d/a	Pair distances after slip									
		0.707	1.0	1.225	1.414	1.581	1.732	1.871	2.0	2.121	2.236
Pair distances before slip	0.707	-	1	1	0	0	0	0	0	0	0
	1.0	1	-	1	0	1	0	0	0	0	0
	1.225	1	1	-	2	3	1	1	0	0	0
	1.414	0	0	2	-	2	0	2	0	0	0
	1.581	0	1	3	2	-	0	3	2	3	1
	1.732	0	0	1	0	0	-	4	0	0	0
	1.871	0	0	1	2	3	4	-	0	8	4
	2.0	0	0	0	0	2	0	0	-	2	0
	2.121	0	0	0	0	3	0	8	2	-	7
	2.236	0	0	0	0	1	0	4	0	7	-

(a) $a/2[1\bar{1}0]$ slip along (111) plane in fcc.

	d/a \ d'/a	Pair distances after slip									
		0.866	1.0	1.414	1.658	1.732	2.0	2.179	2.236	2.449	2.598
Pair distances before slip	0.866	-	1	1	0	0	0	0	0	0	0
	1.0	1	-	0	1	0	0	0	0	0	0
	1.414	1	0	-	4	0	0	1	0	0	0
	1.658	0	1	4	-	2	2	0	4	1	0
	1.732	0	0	0	2	-	0	2	0	0	0
	2.0	0	0	0	2	0	-	0	0	0	2
	2.179	0	0	1	0	2	0	-	6	6	0
	2.236	0	0	0	4	0	0	6	-	0	6
	2.449	0	0	0	1	0	0	6	0	-	6
	2.598	0	0	0	0	0	2	0	6	6	-

(b) $a/2[111]$ slip along (110) plane in bcc.

Table 1: Structure factors $n_{dd'}$ for pairs of normalized pair distances (d,d') for full slip in fcc and bcc crystals respectively.

Due to translational symmetry, there are $\mathbf{N}_a$ identical terms in the $\sum_k$ in Equation 21 where $\mathbf{N}_a = \rho_G \rho_L A_{slip}$ is the total number of atom sites along the slipped area A_{slip} and ρ_G and ρ_L are the atomic line densities along the glide and dislocation line directions, respectively. The average energy change due to full slip can then be written as

$$\langle \Delta E_{ss,f} \rangle = -\frac{1}{2}\mathbf{N}_a \sum_{p,q} c_p c_q \sum_d V_{pq}^{eff}(d) \left(\sum_{\substack{d' \\ d' \neq d}} \lambda_{pq}(d') n_{d'd} - \lambda_{pq}(d) M_d \right) \tag{22}$$

Since $n_{dd'} = n_{d'd}$ for slip by b and $\mathbf{N}_a = \rho_G \rho_L A_{slip}$, we combine Equations 20 and 22 and convert to the Warren-Cowley SRO parameters to obtain the athermal strengthening τ_A as

$$\tau_A = \frac{\rho_L \rho_G}{2b} \sum_{p,q} c_p c_q \sum_d V_{pq}^{eff}(d) \left(\sum_{\substack{d' \\ d' \neq d}} \alpha_{pq}(d') n_{d'd} - \alpha_{pq}(d) M_d \right) \tag{23}$$

With $\rho_G \rho_L = 2/\sqrt{3}b^2$ for slip on $\{111\}$ planes in fcc crystals and $\rho_G \rho_L = 3/(2\sqrt{2})b^2$ for slip on $\{110\}$ planes in bcc crystals [6], the temperature-independent (athermal) strengthening τ_A due to SRO is

$$\tau_A = \begin{cases} \frac{1}{\sqrt{3}b^3} \sum_d \sum_{\substack{p,q \\ p \neq q}} c_p c_q V_{pq}^{eff}(d) \left(\sum_{\substack{d' \\ d' \neq d}} \alpha_{pq}(d') n_{dd'} - \alpha_{pq}(d) M_d \right) & \text{fcc} \\ \frac{3}{4\sqrt{2}b^3} \sum_d \sum_{\substack{p,q \\ p \neq q}} c_p c_q V_{pq}^{eff}(d) \left(\sum_{\substack{d' \\ d' \neq d}} \alpha_{pq}(d') n_{dd'} - \alpha_{pq}(d) M_d \right) & \text{bcc} \end{cases} \tag{24}$$

τ_A is always positive for physical combinations of solute interactions and the associated SRO, since slip always disrupts SRO and so always incurs an energy penalty. Eqs. 24 are the first major results of this paper, expressing the athermal strengthening in an alloy with SRO solely in terms of the EPIs, the Warren-Cowley SRO parameters, and the alloy concentration and lattice parameter.

In the special case where the atoms in the alloy interact only with their first neighbours at distance d_1 and the Warren-Cowley SRO parameters are also non-zero only for the first neighbours, τ_A reduces to

$$\tau_A = \begin{cases} -\frac{2}{\sqrt{3}b^3}\sum_{\substack{p,q\\p\neq q}} c_p c_q \alpha_{pq}(d_1) V_{pq}^{eff}(d_1) & \text{for fcc} \\ -\frac{3}{2\sqrt{2}b^3}\sum_{\substack{p,q\\p\neq q}} c_p c_q \alpha_{pq}(d_1) V_{pq}^{eff}(d_1) & \text{for bcc} \end{cases} \tag{25}$$

Flinn [10] derived this result for fcc binary alloys in terms of EPIs, (but note that Flinn's EPIs are defined as $-V_{pq}^{eff}(d)/2$ in the notation used here). Recently Antillon et. al [23] derived the same result for fcc in terms of binding energies $U^{p,q} = -V_{pq}^{eff}/2$. For the case where atomic interactions and correlations extend only up to the second nearest neighbours d_2, τ_A is

$$\tau_A = \begin{cases} \frac{1}{\sqrt{3}b^3}\sum_{\substack{p,q\\p\neq q}} c_p c_q \left(\alpha_{pq}(d_1)\Big(-2V_{pq}^{eff}(d_1) + V_{pq}^{eff}(d_2)\Big) + \alpha_{pq}(d_2)\Big(V_{pq}^{eff}(d_1) - 3V_{pq}^{eff}(d_2)\Big)\right) & \text{for fcc} \\ \frac{3}{4\sqrt{2}b^3}\sum_{\substack{p,q\\p\neq q}} c_p c_q \left(\alpha_{pq}(d_1)\Big(-2V_{pq}^{eff}(d_1) + V_{pq}^{eff}(d_2)\Big) + \alpha_{pq}(d_2)\Big(V_{pq}^{eff}(d_1) - 2V_{pq}^{eff}(d_2)\Big)\right) & \text{for bcc} \end{cases} \tag{26}$$

This result was derived by Mohri et. al [11] for fcc alloys.

The average stable stacking fault energy also changes due to SRO. This is analyzed in Appendix A following a similar derivation path.

4.2. Strengthening due to fluctuations

4.2.1. Recap of basic theory

The low-energy wavy structure of the dislocation is determined by the standard deviation of the potential energy change $\sigma_{\Delta E_p}(\zeta, w)$ [1–5]. Here, w is now the amplitude of waviness around a given average dislocation line location, independent of the prior total slip of the dislocation. We summarize the main features of the theory to show how $\sigma_{\Delta E_p}(\zeta, w)$ enters in the formulation so that we can subsequently include SRO through its effects on $\sigma_{\Delta E_p}(\zeta, w)$.

The total energy of a long dislocation of length L with waviness scales $\{\zeta, w\}$ is a combination of the energy cost of increasing the dislocation length relative to a straight dislocation, which is related to the dislocation line tension Γ, and the potential energy gain due to pinning at favourable solute environments,

$$\Delta E_{\text{tot}}(\zeta, w) = \left[\Gamma\left(\frac{w^2}{2\zeta}\right) - \sigma_{\Delta E_{\text{p}}}(\zeta, w)\right]\left(\frac{L}{2\zeta}\right) \tag{27}$$

The fluctuation in potential energy change $\sigma_{\Delta E_{\text{p}}}(\zeta, w)$ can be written as

$$\sigma_{\Delta E_{\text{p}}}(\zeta, w) = (\rho_L \zeta)^{1/2}\, \Delta\widetilde{E}_{\text{p}}(w) \tag{28}$$

The quantity $\rho_L \zeta = \mathbf{N}_l$ is the number of atomic sites along the gliding dislocation line segment. The above total energy is then minimized with respect to ζ and w to yield the characteristic (minimum energy) waviness scales ζ_c and w_c. ζ_c is derived as

$$\zeta_c = \left(\frac{4\Gamma^2 w_c^4}{\rho_L \Delta\widetilde{E}_{\text{p}}^2(w_c)}\right)^{\frac{1}{3}} \tag{29}$$

while w_c is the solution of

$$\frac{\partial \Delta\widetilde{E}_{\text{p}}^2(w)}{\partial w} = \frac{\Delta\widetilde{E}_{\text{p}}^2(w)}{w} \tag{30}$$

The dislocation segments of length ζ_c reside in low-energy environments and face high-energy environments at a typical distance w_c along the glide plane. The system energy versus dislocation position is approximated with sinusoidal function [2] and the associated energy barrier faced by the local segments of length ζ_c is then derived as

$$\Delta E_b = 1.467 \left(\rho_L w_c^2 \Gamma \Delta \widetilde{E}_{\mathrm{p}}^2(w_c) \right)^{\frac{1}{3}} \tag{31}$$

To glide the dislocation at zero temperature requires an applied stress $\Delta\tau_{y0}$ *in addition to the athermal stress* τ_A that reduces the above barrier to zero and is derived as

$$\Delta\tau_{y0} = \frac{\pi}{2} \frac{\Delta E_b}{b\zeta_c w_c} = 1.45 \left(\frac{\rho_L^2 \, \Delta \widetilde{E}_{\mathrm{p}}^4(w_c)}{\Gamma b^3 w_c^5} \right)^{\frac{1}{3}} \tag{32}$$

At finite temperatures, the dislocation can move by thermal activation over the energy barrier. An applied stress reduces the barrier, and at low temperatures and applied stress $\tau > \tau_A$, the barrier is well-represented as

$$\Delta E(\tau) \approx \Delta E_b \left(1 - \frac{\tau - \tau_A}{\Delta\tau_{y0}} \right)^{\frac{3}{2}} \tag{33}$$

The rate of motion over the barrier is given by the Arrhenius law for thermal activation, and inversion of that model then leads to the yield stress as a function of temperature T and strain-rate $\dot{\varepsilon}$ of

$$\tau_y(T, \dot{\varepsilon}) = \tau_A + \Delta\tau_{y0} \left[1 - \left(\frac{k_{\mathrm{B}} T}{\Delta E_b} \ln \left(\frac{\dot{\varepsilon}_0}{\dot{\varepsilon}} \right) \right)^{\frac{2}{3}} \right] \tag{34}$$

where $\dot{\varepsilon}_0 \sim 10^4/s$ is a reference strain rate and and k_{B} is Boltzmann's constant respectively. The above single-scale waviness analysis is valid at low T (high strength) while a multi-scale waviness becomes relevant at higher T (lower strength) [38], but the above result is sufficient for the analysis here.

From the above results, we see that it is the normalized variance $\Delta\widetilde{E}_{\mathrm{p}}^2$ in the energy fluctuations that is the key quantity determining the thermally-activated strengthening in the alloy. The strengthening by SRO then requires the evaluation of $\Delta\widetilde{E}_{\mathrm{p}}^2$ in the presence of SRO. The variance $\sigma^2_{\Delta E_{\mathrm{p}}}(\zeta, w) = (\rho_L \zeta) \Delta\widetilde{E}_{\mathrm{p}}^2(w)$ can be decomposed as follows [6]

$$\sigma^2_{\Delta E_{\mathrm{p}}} = \begin{cases} \sigma^2_{\Delta E_{sd}} + \sigma^2_{\Delta E_{ss,f}} + \mathrm{cov}\left(\Delta E_{sd}, \Delta E_{ss,f}\right) & \text{compact core} \\ \sigma^2_{\Delta E_{sd}} + 2\sigma^2_{\Delta E_{ss,p}} + \mathrm{cov}\left(\Delta E_{sd}, \Delta E_{ss,p+}\right) + \mathrm{cov}\left(\Delta E_{sd}, \Delta E_{ss,p-}\right) & \\ + \mathrm{cov}\left(\Delta E_{ss,p+}, \Delta E_{ss,p-}\right) & \text{split core, } w < d_p \\ \sigma^2_{\Delta E_{sd}} + \sigma^2_{\Delta E_{ss,f}} + 2\sigma^2_{\Delta E_{ss,p}} + \mathrm{cov}\left(\Delta E_{sd}, \Delta E_{ss,p+}\right) + \mathrm{cov}\left(\Delta E_{sd}, \Delta E_{ss,p-}\right) & \\ + \mathrm{cov}\left(\Delta E_{sd}, \Delta E_{ss,f}\right) + \mathrm{cov}\left(\Delta E_{ss,f}, \Delta E_{ss,p+}\right) + \mathrm{cov}\left(\Delta E_{ss,f}, \Delta E_{ss,p-}\right) & \\ + \mathrm{cov}\left(\Delta E_{ss,p+}, \Delta E_{ss,p-}\right) & \text{split core, } w > d_p \end{cases} \tag{35}$$

where $\sigma_{\Delta E_{ss,p+}} = \sigma_{\Delta E_{ss,p-}} \equiv \sigma_{\Delta E_{ss,p}}$. The covariance $\mathrm{cov}\left(\Delta E_{sd}, \Delta E_{ss,p+}\right) = \langle \Delta E_{sd} \Delta E_{ss,p+} \rangle$ since $\langle \Delta E_{sd} \rangle = 0$. Substituting ΔE_{sd} and $\Delta E_{ss,p+}$ from Equations 17 and 18b, we have

$$\begin{aligned} \mathrm{cov}\left(\Delta E_{sd}, \Delta E_{ss,p+}\right) = &-\frac{1}{2} \sum_{i,k,l} \sum_{n,p,q} \langle s_i^n s_k^p s_l^q \rangle \left(U_{sd}^n(x_i - w, y_i) - U_{sd}^n(x_i, y_i) \right) \left(V_{pq}^{eff}(d_{kl}^p) - V_{pq}^{eff}(d_{kl}) \right) \\ &+ \frac{1}{2} \sum_{i,j} \sum_{n,p} \langle s_i^n s_j^p \rangle \left(U_{sd}^n(x_i - w, y_i) - U_{sd}^n(x_i, y_i) \right) \Delta\varepsilon_j^p \end{aligned} \tag{36}$$

Similarly, using Equations 17 and 18c, one can deduce

$$\begin{aligned} \mathrm{cov}\left(\Delta E_{sd}, \Delta E_{ss,p-}\right) = &\frac{1}{2} \sum_{i,k,l} \sum_{n,p,q} \langle s_i^n s_k^p s_l^q \rangle \left(U_{sd}^n(x_i - w, y_i) - U_{sd}^n(x_i, y_i) \right) \left(V_{pq}^{eff}(d_{kl}^p) - V_{pq}^{eff}(d_{kl}) \right) \\ &- \frac{1}{2} \sum_{i,j} \sum_{n,p} \langle s_i^n s_j^p \rangle \left(U_{sd}^n(x_i - w, y_i) - U_{sd}^n(x_i, y_i) \right) \Delta\varepsilon_j^p \end{aligned} \tag{37}$$

From the above expansions of the covariances, it is clear that $\mathrm{cov}\left(\Delta E_{sd},\Delta E_{ss,p+}\right)=-\mathrm{cov}\left(\Delta E_{sd},\Delta E_{ss,p-}\right)$. In a similar fashion it can be shown that $\mathrm{cov}\left(\Delta E_{ss,f},\Delta E_{ss,p+}\right)=-\mathrm{cov}\left(\Delta E_{ss,f},\Delta E_{ss,p-}\right)$. These terms therefore cancel in Equation 35 and need not be calculated. Furthermore, the quantity $\mathrm{cov}\left(\Delta E_{ss,p+},\Delta E_{ss,p-}\right)=0$ since the newly created and annihilated stacking faults are separated by $|d_p-w|$ (which in all practical cases is greater than the range of typical EPIs). Considering the above simplifications, we can rewrite Equation 35 as

$$\sigma^2_{\Delta E_\mathrm{p}}=\begin{cases}\sigma^2_{\Delta E_{sd}}+\sigma^2_{\Delta E_{ss,f}}+\mathrm{cov}\left(\Delta E_{sd},\Delta E_{ss,f}\right) & \text{compact core}\\ \sigma^2_{\Delta E_{sd}}+2\sigma^2_{\Delta E_{ss,p}} & \text{split core, } w<d_p\\ \sigma^2_{\Delta E_{sd}}+\sigma^2_{\Delta E_{ss,f}}+2\sigma^2_{\Delta E_{ss,p}}+\mathrm{cov}\left(\Delta E_{sd},\Delta E_{ss,f}\right) & \text{split core, } w>d_p\end{cases} \tag{38}$$

The variances are assessed in subsequent sections for alloys with SRO. The covariance $\mathrm{cov}(\Delta E_{sd},\Delta E_{ss,f})$ in Equation 38 is negligible compared to the variances and will be ignored henceforth; this is justified in Appendix C.

4.2.2. Strengthening from fluctuations due to solute-dislocation interactions

The variance in ΔE_{sd} due to solute-dislocation interactions is $\sigma^2_{\Delta E_{sd}}=\langle\Delta E^2_{sd}\rangle-\langle\Delta E_{sd}\rangle^2=\langle\Delta E^2_{sd}\rangle$ since $\langle\Delta E_{sd}\rangle=0$. Recalling Equation 17, for a given solute configuration we have

$$\Delta E^2_{sd}=\sum_{i,j,n,m}s^n_i s^m_j\Delta U^n_{sd,i}(w)\Delta U^m_{sd,j}(w) \tag{39}$$

where $\Delta U^n_{sd,i}(w)=U^n_{sd}(x_i-w,y_i)-U^n_{sd}(x_i,y_i)$. Averaging over all solute realizations using $\langle s^n_i s^m_j\rangle=\delta_{ij}\delta_{nm}c_n+(1-\delta_{ij})\,\lambda^{ij}_{nm}c_n c_m$, we obtain

$$\begin{aligned}\sigma^2_{\Delta E_{sd}}=&\sum_n c_n\sum_i\left(\Delta U^n_{sd,i}(w)\right)^2\\&+\sum_{\substack{i,j\\ i\neq j}}\sum_n c_n\Delta U^n_{sd,i}(w)\sum_m c_m\Delta U^m_{sd,j}(w)\;\lambda^{ij}_{nm}\end{aligned} \tag{40}$$

The first term is precisely the expression arising in the random alloy because the second term is zero when $\lambda^{ij}_{nm}=1$ since $\sum_n c_n\Delta U^n_{sd,i}(w)=0$ by definition of the average alloy through which the interactions are determined. The variance can then be rewritten in terms of the Warren-Cowley parameters α^{ij}_{nm} as

$$\begin{aligned}\sigma^2_{\Delta E_{sd}}=&\sum_n c_n\sum_i\left(\Delta U^n_{sd,i}(w)\right)^2\\&-\sum_{\substack{i,j\\ i\neq j}}\sum_n c_n\Delta U^n_{sd,i}(w)\sum_m c_m\Delta U^m_{sd,j}(w)\;\alpha^{ij}_{nm}\end{aligned} \tag{41}$$

Furthermore, since $\Delta U^n_{sd,i}(w)$ only depends on the x and y coordinates (Equation 39), a single site at any z_i is representative of all $\mathbf{N}_l=\zeta\rho_L$ sites at positions (x_i,y_i) parallel to the dislocation line. We can thus partition all sites i into subsets $[i]=\{$all sites k such that $x_k=x_i$ and $y_k=y_i\;\}$ and factor out $\mathbf{N}_l$ to arrive at

$$\begin{aligned}\Delta\widetilde{E}^2_{\mathrm{p},sd}=\frac{\sigma^2_{\Delta E_{sd}}}{\mathbf{N}_l}=\frac{\sigma^2_{\Delta E_{sd}}}{\zeta\rho_L}=&\sum_n c_n\sum_{[i]}\left(\Delta U^n_{sd,i}(w)\right)^2\\&-\sum_{[i]}\sum_n c_n\Delta U^n_{sd,i}(w)\sum_{\substack{j\\ j\neq i}}\sum_m c_m\Delta U^m_{sd,j}(w)\;\alpha^{ij}_{nm}\end{aligned} \tag{42}$$

where $\sum_{[i]}$ is a sum over only the projected in-plane sites (x_i,y_i) in one periodic distance along the dislocation line direction.

The variance due to solute/dislocation interactions thus consists of the contribution obtained in the random alloy plus an additional contribution that scales linearly with the SRO parameters and is second-order in the composition. *Importantly, the second term involving SRO can be positive or negative. Thus, SRO can increase or decrease the alloy strength relative to random alloy counterpart, even though τ_A is always positive.* We will simplify and discuss this result further in Section 5. The general result of Equation 42, and its implications, is the second main result of this paper.

4.2.3. Strengthening from fluctuations due to solute-solute interactions

The variance of $\Delta E_{ss,f}$ is given by $\sigma^2_{\Delta E_{ss,f}} = \langle \Delta E^2_{ss,f} \rangle - \langle \Delta E_{ss,f} \rangle^2$ and similarly for $\sigma^2_{\Delta E_{ss,p}}$. The mean $\langle \Delta E_{ss,f} \rangle / A_{slip}$ equals γ_{SRO} (recall Section 4.1), while $\langle \Delta E_{ss,p} \rangle / A_{slip}$ is the stacking fault energy γ_{ssfe} (see Appendix A). With atom sites and types below the slip plane denoted by i,k and u,p, respectively, and atom sites and types above the slip plane denoted by j,l and v,q, respectively, the quantity $\Delta E^2_{ss,f}$ follows from Equation 18a as

$$\Delta E^2_{ss,f} = \frac{1}{4} \sum_{k,l} \sum_{p,q} s^p_k s^q_l \left(V^{eff}_{pq}(d^f_{kl}) - V^{eff}_{pq}(d_{kl}) \right) \sum_{i,j} \sum_{u,v} s^u_i s^v_j \left(V^{eff}_{uv}(d^f_{ij}) - V^{eff}_{uv}(d_{ij}) \right) \tag{43}$$

and the quantity $\Delta E^2_{ss,p}$ follows from Equation 18b) as

$$\begin{aligned} \Delta E^2_{ss,p} = & \frac{1}{4} \sum_{k,l} \sum_{p,q} s^p_k s^q_l \left(V^{eff}_{pq}(d^p_{kl}) - V^{eff}_{pq}(d_{kl}) \right) \sum_{i,j} \sum_{u,v} s^u_i s^v_j \left(V^{eff}_{uv}(d^p_{ij}) - V^{eff}_{uv}(d_{ij}) \right) \\ & - \sum_{k,l} \sum_{p,q} s^p_k s^q_l \left(V^{eff}_{pq}(d^p_{kl}) - V^{eff}_{pq}(d_{kl}) \right) \sum_{i} \sum_{u} s^u_i \Delta \varepsilon^u_i \\ & + \frac{1}{4} \sum_{k} \sum_{p} s^p_k \Delta \varepsilon^p_k \sum_{i} \sum_{u} s^u_i \Delta \varepsilon^u_i \end{aligned} \tag{44}$$

For full slip, averaging $\Delta E^2_{ss,f}$ over all statistical realization of the alloy involves the expectation $\langle s^p_k s^q_l s^u_i s^v_j \rangle$ which can be expressed, using Equations 1, 3 and 5, as

$$\begin{aligned} \langle s^p_k s^q_l s^u_i s^v_j \rangle = & \delta_{ik}\delta_{up}\delta_{jl}\delta_{vq}\lambda^{kl}_{pq} c_p c_q + \delta_{ik}\delta_{up}(1-\delta_{jl})\lambda^{kjl}_{pvq} c_p c_v c_q \\ & + (1-\delta_{ik})\delta_{jl}\delta_{vq}\lambda^{ikl}_{upq} c_u c_p c_q + (1-\delta_{ik})(1-\delta_{jl})\lambda^{ijkl}_{uvpq} c_u c_v c_p c_q \end{aligned} \tag{45}$$

After considerable algebra, we obtain

$$\begin{aligned} \langle \Delta E^2_{ss,f} \rangle = & \frac{1}{4} \sum_{p,q} c_p c_q \sum_{k,l} \lambda^{kl}_{pq} \left(V^{eff}_{pq}(d^f_{kl}) - V^{eff}_{pq}(d_{kl}) \right)^2 \\ & + \frac{1}{2} \sum_{p,v,q} c_p c_v c_q \sum_{\substack{k,j,l \\ j \neq l}} \lambda^{kjl}_{pvq} \left(V^{eff}_{pq}(d^f_{kl}) - V^{eff}_{pq}(d_{kl}) \right) \left(V^{eff}_{pv}(d^f_{kj}) - V^{eff}_{pv}(d_{kj}) \right) \\ & + \frac{1}{4} \sum_{u,v,p,q} c_u c_v c_p c_q \sum_{\substack{i,j,k,l \\ i \neq k \\ j \neq l}} \lambda^{ijkl}_{uvpq} \left(V^{eff}_{pq}(d^f_{kl}) - V^{eff}_{pq}(d_{kl}) \right) \left(V^{eff}_{uv}(d^f_{ij}) - V^{eff}_{uv}(d_{ij}) \right) \end{aligned} \tag{46}$$

where the manipulations use the fact that, for Bravais lattices like fcc and bcc, the coordination of lattice sites on either side of the slip plane is the same. Expressing Equation 46 in terms of the WC SRO parameters, we have

$$\begin{aligned} \langle \Delta E^2_{ss,f} \rangle = & \langle \Delta E^2_{ss,f} \rangle_{\text{random alloy}} \\ & - \frac{1}{4} \sum_{p,q} c_p c_q \sum_{k,l} \alpha^{kl}_{pq} \left(V^{eff}_{pq}(d^f_{kl}) - V^{eff}_{pq}(d_{kl}) \right)^2 \\ & - \frac{1}{2} \sum_{p,v,q} c_p c_v c_q \sum_{\substack{k,j,l \\ j \neq l}} \alpha^{kjl}_{pvq} \left(V^{eff}_{pq}(d^f_{kl}) - V^{eff}_{pq}(d_{kl}) \right) \left(V^{eff}_{pv}(d^f_{kj}) - V^{eff}_{pv}(d_{kj}) \right) \\ & - \frac{1}{4} \sum_{u,v,p,q} c_u c_v c_p c_q \sum_{\substack{i,j,k,l \\ i \neq k \\ j \neq l}} \alpha^{ijkl}_{uvpq} \left(V^{eff}_{pq}(d^f_{kl}) - V^{eff}_{pq}(d_{kl}) \right) \left(V^{eff}_{uv}(d^f_{ij}) - V^{eff}_{uv}(d_{ij}) \right) \end{aligned} \tag{47}$$

where the last three terms are the additional contributions to the fluctuations due to SRO. Examining the above result, we see that positive α^{kl}_{pq} makes the second term in Equation 47 negative, which decreases $\langle \Delta E^2_{ss,f} \rangle$ and contributes to a decrease in the strength relative to the random alloy. As found for the solute-dislocation contribution, it is thus again possible that SRO decreases alloy strength rather than increasing it. However, the full result requires information on 3 and 4 particle correlations.

Comparing Equations 43 and 44 we can see the first term in the latter only differs in d_{kl}^{p}. Therefore the first term in $\langle \Delta E_{ss,p}^2 \rangle$ will have the same form as Equation 47 for $\langle \Delta E_{ss,f}^2 \rangle$, with d_{kl}^{p} instead of d_{kl}^{f}. After averaging the other two terms in Equation 44 we obtain $\langle \Delta E_{ss,p}^2 \rangle$ in terms of WC-SRO parameters as

$$
\begin{aligned}
\langle \Delta E_{ss,p}^2 \rangle = {} & \langle \Delta E_{ss,p}^2 \rangle_{\text{random alloy}} \\
& - \frac{1}{4} \sum_{p,q} c_p c_q \sum_{k,l} \alpha_{pq}^{kl} \left(V_{pq}^{eff}(d_{kl}^{p}) - V_{pq}^{eff}(d_{kl}) \right)^2 \\
& - \frac{1}{2} \sum_{p,v,q} c_p c_v c_q \sum_{\substack{k,j,l \\ j \neq l}} \alpha_{pvq}^{kjl} \left(V_{pq}^{eff}(d_{kl}^{p}) - V_{pq}^{eff}(d_{kl}) \right) \left(V_{pv}^{eff}(d_{kj}^{p}) - V_{pv}^{eff}(d_{kj}) \right) \\
& - \frac{1}{4} \sum_{u,v,p,q} c_u c_v c_p c_q \sum_{\substack{i,j,k,l \\ i \neq k \\ j \neq l}} \alpha_{uvpq}^{ijkl} \left(V_{pq}^{eff}(d_{kl}^{p}) - V_{pq}^{eff}(d_{kl}) \right) \left(V_{uv}^{eff}(d_{ij}^{p}) - V_{uv}^{eff}(d_{ij}) \right) \\
& + \sum_{p,q} c_p c_q \sum_{k,l} \alpha_{pq}^{kl} \left(V_{pq}^{eff}(d_{kl}^{p}) - V_{pq}^{eff}(d_{kl}) \right) \Delta\varepsilon_k^{p} \\
& + \sum_{p,v,q} c_p c_v c_q \sum_{\substack{k,j,l \\ j \neq l}} \alpha_{pvq}^{kjl} \left(V_{pq}^{eff}(d_{kl}^{p}) - V_{pq}^{eff}(d_{kl}) \right) \Delta\varepsilon_j^{v} \\
& - \frac{1}{2} \sum_{p,q} c_p c_q \sum_{k,l} \alpha_{pq}^{kl} \Delta\varepsilon_k^{p} \Delta\varepsilon_l^{q} - \frac{1}{2} \sum_{v,q} c_v c_q \sum_{\substack{j,l \\ j \neq l}} \alpha_{vq}^{jl} \Delta\varepsilon_j^{v} \Delta\varepsilon_l^{q}
\end{aligned}
\tag{48}
$$

As discussed earlier, the important quantities for thermally activated strengthening, the variances $\sigma_{\Delta E_{ss,f}}^2$ and $\sigma_{\Delta E_{ss,p}}^2$ (Equation 38), are given by

$$
\sigma_{\Delta E_{ss,f}}^2 = \langle \Delta E_{ss,f}^2 \rangle - \langle \Delta E_{ss,f} \rangle^2 = \langle \Delta E_{ss,f}^2 \rangle - (\gamma_{SRO}\, A_{slip})^2 \quad \text{(Using Equation 20)and} \tag{49}
$$

$$
\sigma_{\Delta E_{ss,p}}^2 = \langle \Delta E_{ss,p}^2 \rangle - \langle \Delta E_{ss,p} \rangle^2 = \langle \Delta E_{ss,p}^2 \rangle - (\gamma_{ssfe}\, A_{slip})^2 \quad \text{(Using Equation A.2)} \tag{50}
$$

where γ_{SRO} is derived in Section 4.1 for athermal average strengthening and the stacking fault energy γ_{ssfe} is derived in Appendix A for the case of SRO.

The third and fourth terms in Equations 47 and 48 and also the sixth term in the latter, involve higher-order SRO parameters and are not amenable to simplification or clear interpretation. They may tend to be smaller because they involve three concentrations and multibody correlations, but there are many more terms in the sums that may compensate for these factors. In the limit of small SRO, the correlation functions can be reasonably approximated using the superposition principle, which decomposes the multibody correlations into products of pair correlations (see [39] showing good accuracy for $\alpha < 0.2$ in many cases). With the superposition approximation and small SRO, the multibody correlation functions can be expanded to first order in α as

$$
\begin{aligned}
\alpha_{pvq}^{kjl} &\approx \alpha_{pv}^{kj} + \alpha_{vq}^{jl} + \alpha_{pq}^{kl} \\
\alpha_{uvpq}^{ijkl} &\approx \alpha_{uv}^{ij} + \alpha_{pq}^{kl} + \alpha_{vp}^{jk} + \alpha_{uq}^{il} + \alpha_{vq}^{jl} + \alpha_{up}^{ik}.
\end{aligned}
\tag{51}
$$

However, we are not able to find any useful simplifications even in this limit.

The analytic formulation presented above is developed in the same spirit as the previous analysis of random alloys in Ref. [6]. However the equations are quite unwieldy, owing to the higher-order correlation functions. In Section 5.2, we have therefore provided an alternative computational route for calculation the variance quantities that is easy to implement if suitable interatomic potentials or first-principles methods are available. That computational route also gives more flexibility in terms of considering complex many-body solute-solute interactions and multiple site correlations, but always at the cost of more computational expense.

5. Reductions to practice

The results in the previous section for the contributions to strengthening due to fluctuations are complete but unwieldy. Here, we thus introduce the linear elasticity approximation of Varvenne et al. [3] for the

solute-dislocation interactions and examine the effects of SRO on the solute-dislocation contributions to strengthening. We then discuss computational strategies to avoid having to analytically evaluate the solute-solute fluctuation term, and this approach will also yield the energy γ_{SRO} that determines the athermal strengthening.

5.1. Strengthening due to solute-dislocation interactions

We focus on the solute-dislocation interaction effects for two reasons. First, the analysis is tractable in a fairly general context, as shown below. Second, and more importantly, assuming a random alloy, the solute-dislocation interactions alone have been successful in predicting the strengthening of many different HEAs, thus indicating that this contribution is dominant [4, 5]. The most significant effects of SRO are thus expected to arise through their effects on the (dominant) solute-dislocation interaction contributions. The additional athermal strengthening that is always created by SRO can also be non-negligible, and perhaps dominant at high temperatures where solute-dislocation strengthening is greatly reduced. The fluctuations due to solute-solute interactions likely play a smaller overall role, as shown for a few fcc and bcc random alloys in the absence of SRO in Refs. [6, 40].

5.1.1. Elasticity approximation

The solute-dislocation interaction energies U^n_{sd} can rarely be computed by direct atomistic simulations. First-principles calculations are feasible only for dilute binary alloys. Calculations for HEAs describable by EAM interatomic potentials can take advantage of the ability to create a dislocation in the "average alloy" [41] into which the constituent solute atoms can be introduced to compute the U^n_{sd}. However, EAM potentials are rarely quantitative for real alloys, and so serve mainly as model systems. Due to these various limitations, Varvenne et al. proposed to estimate the U^n_{sd} using linear elasticity as

$$U^n_{sd,i} = -p(x_i, y_i)\Delta V_n \tag{52}$$

where $p(x_i, y_i)$ is the pressure at atomic site i due to the dislocation line at the origin and ΔV_n is the misfit volume of a type-n solute in the alloy. Denoting the change in pressure at site i after dislocation glide by w as $\Delta p_i(w) = p(x_i - w, y_i) - p(x_i, y_i)$, the variance for the solute-dislocation interaction term in Equation 42 can be rewritten as

$$\begin{aligned}\Delta\widetilde{E}^2_{\mathrm{p},sd} = &\left(\sum_n c_n \Delta V_n^2\right)\left(\sum_{[i]} \Delta p_i^2(w)\right) \\ &- \sum_{n,m} c_n c_m \Delta V_n \Delta V_m \sum_{[i]} \sum_{\substack{j \\ j\neq i}} \Delta p_i(w)\Delta p_j(w)\ \alpha^{ij}_{nm}\end{aligned} \tag{53}$$

It has been demonstrated in the context of random alloys that elastic anisotropy has small influence on alloy strength and is best-captured by using the Voigt-averaged elastic constants [42]. Therefore, following the analysis of Varvenne et al. [3], for an elastically isotropic alloy with (Voigt-averaged) shear modulus μ and Poisson's ratio ν, the dependence of $\Delta p_i(w)$ on the elastic constants can be factored out. The variance in energy change due to solute-dislocation interaction is then reduced to the form

$$\begin{aligned}\Delta\widetilde{E}^2_{\mathrm{p},sd}(w) = &\left(\mu \cdot \frac{1+\nu}{1-\nu}\right)^2 \Bigg[\sum_n c_n \Delta V_n^2\, A(w) \\ &+ \sum_{n,m>n} c_n c_m \left(\Delta V_n - \Delta V_m\right)^2 \Bigg(12\, B(w)\ \alpha_{nm}(1^{\text{st}}\ \text{NN}) + 6\, C(w)\ \alpha_{nm}(2^{\text{nd}}\ \text{NN}) \\ &+ 24\, D(w)\ \alpha_{nm}(3^{\text{rd}}\ \text{NN}) + 12\, E(w)\ \alpha_{nm}(4^{\text{th}}\ \text{NN}) + \ldots\Bigg)\Bigg] \quad \text{for FCC alloys}\end{aligned} \tag{54a}$$

$$\begin{aligned}\Delta\widetilde{E}^2_{\mathrm{p},sd}(w) = &\left(\mu \cdot \frac{1+\nu}{1-\nu}\right)^2 \Bigg[\sum_n c_n \Delta V_n^2\, A(w) \\ &+ \sum_{n,m>n} c_n c_m \left(\Delta V_n - \Delta V_m\right)^2 \Bigg(8\, B(w)\ \alpha_{nm}(1^{\text{st}}\ \text{NN}) + 6\, C(w)\ \alpha_{nm}(2^{\text{nd}}\ \text{NN}) \\ &+ 12\, D(w)\ \alpha_{nm}(3^{\text{rd}}\ \text{NN}) + 24\, E(w)\ \alpha_{nm}(4^{\text{th}}\ \text{NN}) + \ldots\Bigg)\Bigg] \quad \text{for BCC alloys}\end{aligned} \tag{54b}$$

where the coefficients $A(w), B(w), \ldots$ are all positive (see Figure 3 below) functions of the glide distance w and depend on the spatial distribution of the pressure field. The coefficients are derived in Appendix B, with their analytic forms presented in Equations A.10 and A.11 for fcc and bcc alloys respectively.

Antillon et al. [23] developed a related expression that accounts only for first-neighbor SRO and that also neglects spatial correlations in the pressure field that eliminate possible changes in w_c due to SRO. Within those limits, the form of Eqs. 19–20 in Ref. [23] agrees with our derived theory but the numerical prefactor is incorrect. Eqs. 19–20 in Ref. [23] appear different than our equations above because Antillon et al. did not take advantage of the sum rule of our Equation 11. Application of the sum rule reveals that SRO strengthening only depends on differences in misfit volumes, as can be understood physically. Unfortunately, the form in Antillon et al. then led them to incorrectly state that if either ΔV_n or ΔV_m is zero then the SRO contribution to strengthening from the *nm* pair is zero.

For the special case of a binary alloy with concentrations c and $(1-c)$, misfit volumes ΔV and $-c\Delta V/(1-c)$ respectively (since $\sum_n c_n \Delta V_n = 0$), and WC-SRO parameters α, Equation 53 simplifies, for an fcc alloy, to

$$\Delta\widetilde{E}^2_{\mathrm{p},sd}(w) = \frac{c}{(1-c)}\Delta V^2 \left(\mu \cdot \frac{1+\nu}{1-\nu}\right)^2 \Big[A(w) + 12\,B(w)\;\alpha(1^{\mathrm{st}}\ \mathrm{NN}) + 6\,C(w)\;\alpha(2^{\mathrm{nd}}\ \mathrm{NN}) + 24\,D(w)\;\alpha(3^{\mathrm{rd}}\ \mathrm{NN}) + 12\,E(w)\;\alpha(4^{\mathrm{th}}\ \mathrm{NN}) + \ldots\Big] \tag{55}$$

and similarly for a bcc alloy. The apparent divergence in the limit $c \to 1$ does not exist because $\Delta V \to 0$ in this limit. This limit is the dilute limit of the second element, and so a clearer analytic (and again non-diverging) result would emerge if ΔV is taken as the misfit of the second element in the matrix of the first element. Alternatively, if Vegard's law is used to express the misfit volumes in terms of the two atomic volumes V_{a1} and V_{a2} [43], the prefactor can be written as $c(1-c)(V_{a1}-V_{a2})^2$ that is easily seen to become zero for both $c \to 1$ and $c \to 0$.

There are several insights that can be made from the above results. First, the fluctuating energy must be minimized with respect to w to obtain w_c. Changes to w_c then affect the energy barrier and zero-T flow stress in Equations 31, 32, even if the other quantities do not change. In addition, the contributions to the barrier and flow stress from solute-solute interactions also scale linearly with w_c in the absence of SRO, as shown in Ref. [6]. Hence, even in the presence of SRO, we can expect that solute-solute contributions can be changed if w_c differs from the value in the random alloy. We will analyze the first issue further below, but in general changes to w_c can increase *or* decrease strength.

More importantly, relative to the random alloy, the fluctuations, and hence strength, can decrease if the combination of SRO parameters, misfit volumes, and concentrations in the second term of Equation 54a or 54b is negative. Because the misfit strengthening can be large and dominant in many HEAs, *the alloy strength can be decreased due to SRO even if there is always a positive athermal strengthening.* This is a critical rigorous result emerging from our analysis, which had previously been noted by Antillon et al. [23] based on their approximate analysis and limited simulations.

A reduction in strength due to SRO is predicted particularly in alloys where solute pairs (n,m) are attracted to one another at some distance d ($\alpha_{nm}(d) < 0$) and have large and opposite-signed misfit volumes so that $|\Delta V_n - \Delta V_m|$ is large (see Equations 54a and 54b). Since long-range ordering in many alloys is correlated with atomic size mismatch [44], this situation (attractive, opposite-signed misfit pairs) may be common. This suggests a lowering of strength due to fluctuations that would offset to some degree the positive athermal strengthening, leading to reduced overall effects of SRO on strength. In the limit of formation of a perfectly ordered intermetallic, the fluctuations become zero - the random alloy strengthening is entirely lost - and the strengthening is then only the athermal strengthening related to the shearing energy (anti-phase boundary energy) of the ordered structure. Our results also show that SRO between solute pairs (n,m) with similar misfit volumes have a much smaller effect on strengthening, whether positive or negative, because they have similar interactions with the dislocation pressure field. Making such pairs more or less spatially correlated thus has much smaller effect on the overall strengthening as compared to pairs with opposite-signed misfits.

To further progress toward practical applications and analytic results, the pressure field generated by a dislocation can be modeled by representing the dislocation core structure as a continuous distribution of Burgers vector along the glide plane. Previous work has shown that the Burgers vector distribution can be reasonably characterized in fcc alloys as two Gaussian functions, one for each partial, each with width σ and separated by the partial dissociation distance d_p. Bcc alloys have compact dislocation core, and limited atomistic studies of edge dislocation cores suggest that they can be characterized by a single Gaussian function

with core spreading of $\sigma = 1.333b$. With such a parameterization of the core structure in terms of (σ, d_p), the coefficients $A, B, C, D, \ldots$ can be computed as a function of the parameters σ, d_p, and w. In fcc alloys, it emerges that the coefficients are independent of d_p for $d_p > 9b$, which is a common regime for many fcc HEAs studied to date (all of which have rather low stable stacking fault energies).

Figure 3a shows the coefficients $A(w), B(w), \ldots$ for fcc crystals as functions of w for $\sigma = 1.5b, 2b$ at $d_p (= 15b)$ that covers a range of alloys [6, 42]. All the coefficients have a similar general behavior versus w. The $A(w)$ coefficient is that for the random alloy, and is identical to the quantity g^2_{iso} obtained previously Refs. [6, 42]. For both values of σ, the $B(w)$ coefficient is similar in form but slightly smaller than A (but with a prefactor of 12 equal to the number of first neighbors), while the C, D, E coefficients are all nearly identical. For larger w (not shown), the coefficients are non-monotonic and hence there can be additional solutions for w_c that are relevant at higher temperatures [4, 45] but here we focus on the range of w relevant for the low temperature domain that typically includes room temperature.

Figure 3b shows the coefficients $A(w), B(w), \ldots$ versus w for edge dislocations in bcc alloys with core spreading of $\sigma = 1.333b$, characteristic of the non-dissociated edge core in bcc. All the coefficients including the random term $A(w)$ are 30–40% larger than for fcc, so bcc alloys are intrinsically stronger than fcc. Most important for SRO are the magnitudes of the SRO-related coefficients B, C, D,...relative to A, and these are roughly similar between fcc and bcc so that SRO has roughly similar effects in fcc and bcc alloys.

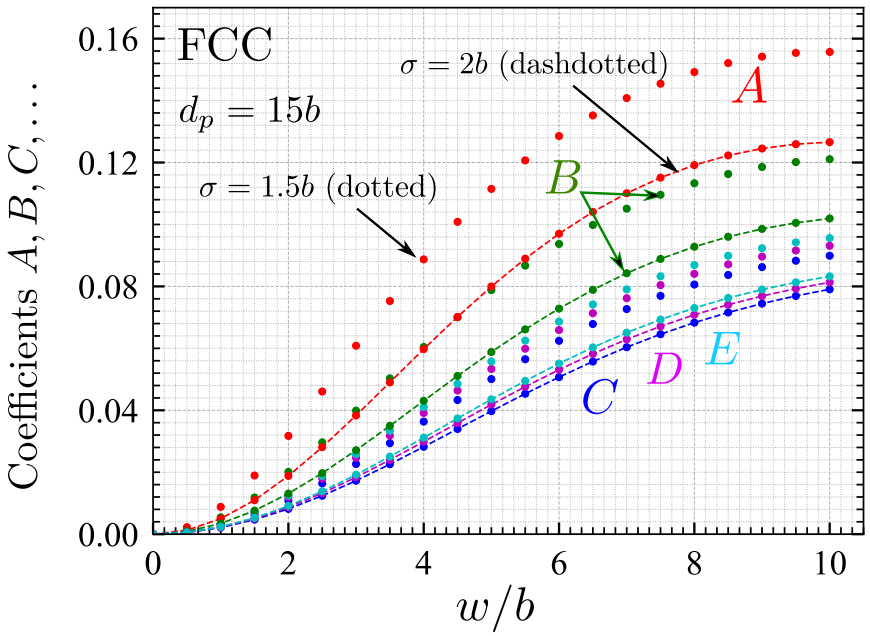

(a) FCC edge dislocation with widely separated Shockley partials

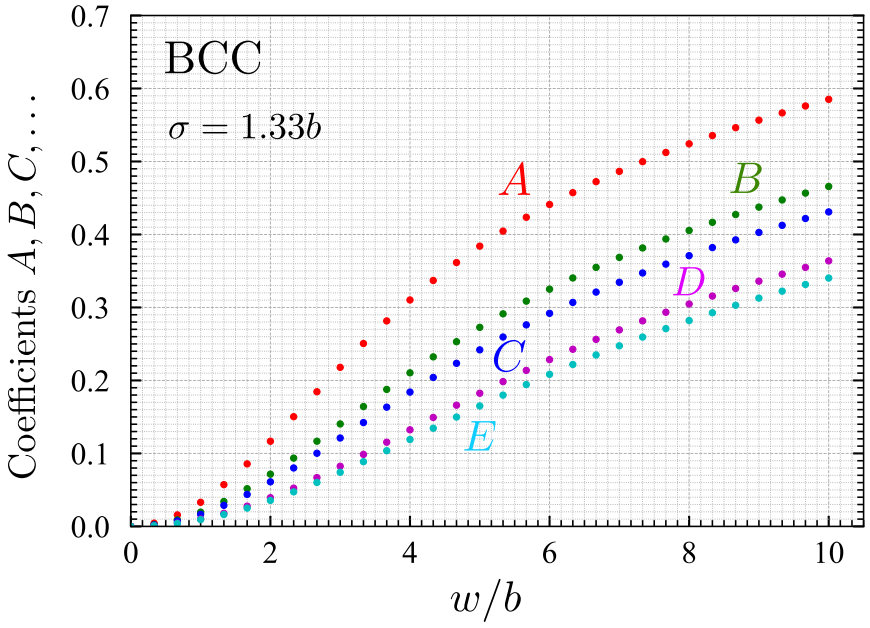

(b) BCC edge dislocation $a/2\langle 111\rangle/\{110\}$ with compact core

Figure 3: Coefficients A, B, C, D, E appearing in Equations 54a and 54b as a function of glide distance w, for edge dislocation in (a) fcc and (b) bcc alloys. Results are presented for two different Shockley partial core widths $\sigma = 1.5b, 2.0b$ for fcc alloys with largely separated Shockley partials $d_p > 10b$. For bcc alloys with compact full dislocation core, results are presented for core width $\sigma = 1.3333b$.

5.1.2. Approximate analytic results

As mentioned above, the final theory predictions require minimization of the total energy with respect to w to obtain w_c, which reduces to the solution of $\frac{\partial \Delta \widetilde{E}_{\mathrm{p}}^2(w)}{\partial w} = \frac{\Delta \widetilde{E}_{\mathrm{p}}^2(w)}{w}$ (Eq. 30). For small SRO, the random alloy value of w_c can be used directly. In general, for a given SRO, the functions $A(w), B(w), \ldots$ shown in Figures 3a, 3b can be used to execute the minimization numerically. Here, we can make analytic progress for small to moderate SRO as follows. Using Equation 54a for multicomponent fcc alloys in Equation 30 and

manipulating, one can deduce that w_c must satisfy

$$\left(A'(w)-\frac{A(w)}{w}\right)\beta_0+12\left(B'(w)-\frac{B(w)}{w}\right)\beta_1+6\left(C'(w)-\frac{C(w)}{w}\right)\beta_2 \\ +24\left(D'(w)-\frac{D(w)}{w}\right)\beta_3+12\left(E'(w)-\frac{E(w)}{w}\right)\beta_4=0 \tag{56}$$

where $A'(w)=dA/dw$ etc. and $\beta_0=\sum_n c_n\Delta V_n^2$ and $\beta_i=\sum_{n,m>n}c_nc_m\left(\Delta V_n-\Delta V_m\right)^2\alpha_{nm}(i^{\text{th}}\text{ NN})$. Note that in the binary limit, $\beta_0=c\Delta V^2/(1-c)$ and $\beta_i/\beta_0=\alpha(i^{\text{th}}\text{ NN})$. For bcc alloys, the fcc coordinations of 12, 6, 24, 12 should be replaced by 8, 6, 12, 24 respectively.

Now let w_c^A be the solution to $A'(w_c^A)-A(w_c^A)/w_c^A=0$, which is the random alloy value ($w_c^A/b=4.5,5.5$ for fcc edge dislocations with $\sigma/b=1.5,2.0$ and $w_c^A/b=4.333$ for bcc edge dislocations with $\sigma/b=1.333$). We then expand the coefficients $A,B,C,\ldots$ to second order in w around w_c^A as

$$\begin{aligned}\bar{A}(w)&\approx A(w_c^A)+A'(w_c^A)(w-w_c^A)+{}^1\!/_2A''(w_c^A)(w-w_c^A)^2\\ \bar{B}(w)&\approx B(w_c^A)+B'(w_c^A)(w-w_c^A)+{}^1\!/_2B''(w_c^A)(w-w_c^A)^2\\ &\vdots\end{aligned} \tag{57}$$

and use these expansions in Equation 56. Using the relation $A'(w_c^A)-A(w_c^A)/w_c^A=0$, we can then solve for w_c as

$$w_c\approx w_c^A\left(1-\frac{12\left(B'(w_c^A)-B(w_c^A)/w_c^A\right)\beta_1+6\left(C'(w_c^A)-C(w_c^A)/w_c^A\right)\beta_2+\ldots}{{}^1\!/_2\,w_c^A\left(A''(w_c^A)\,\beta_0+12\,B''(w_c^A)\,\beta_1+6\,C''(w_c^A)\,\beta_2+\ldots\right)}\right)^{\frac{1}{2}}\quad\text{FCC alloys} \tag{58a}$$

$$w_c\approx w_c^A\left(1-\frac{8\left(B'(w_c^A)-B(w_c^A)/w_c^A\right)\beta_1+6\left(C'(w_c^A)-C(w_c^A)/w_c^A\right)\beta_2+\ldots}{{}^1\!/_2\,w_c^A\left(A''(w_c^A)\,\beta_0+8\,B''(w_c^A)\,\beta_1+6\,C''(w_c^A)\,\beta_2+\ldots\right)}\right)^{\frac{1}{2}}\quad\text{BCC alloys} \tag{58b}$$

The computed values for $w_c^A,A''(w_c^A),B(w_c^A),B'(w_c^A),B''(w_c^A)$ etc. are shown in Table 2 for fcc and bcc edge dislocations. w_c can thus be computed for any specified SRO and misfit parameters. Using the values from the Table, fcc edge dislocations with $\sigma/b=1.5$ have

$$\frac{w_c}{w_c^A}\approx\left(1+\frac{0.03355\,\beta_1+0.02459\,\beta_2+0.09338\,\beta_3+0.04758\,\beta_4+\ldots}{0.0132\,\beta_0+0.0841\,\beta_1+0.01056\,\beta_2+0.0593\,\beta_3+0.0354\,\beta_4+\ldots}\right)^{\frac{1}{2}} \tag{59}$$

and similarly for the bcc edge dislocations with $\sigma/b=1.3333$

$$\frac{w_c}{w_c^A}\approx\left(1+\frac{0.083\,\beta_1+0.072\,\beta_2+0.1932\,\beta_3+0.36257\,\beta_4+\ldots}{0.0417\,\beta_0+0.16584\,\beta_1+0.089\,\beta_2+0.047\,\beta_3+0.029474\,\beta_4+\ldots}\right)^{\frac{1}{2}} \tag{60}$$

With the approximate coefficients $\bar{A},\bar{B},\ldots$ from Equation 57 evaluated at w_c, the energy fluctuation quantity $\Delta\widetilde{E}^2_{\text{p},sd}(w_c)$ is approximated as

$$\Delta\widetilde{E}^2_{\text{p},sd}(w_c)\approx\left(\mu\cdot\frac{1+\nu}{1-\nu}\right)^2\left(\beta_0\,\bar{A}(w_c)+12\,\beta_1\,\bar{B}(w_c)+6\,\beta_2\,\bar{C}(w_c)+24\,\beta_3\,\bar{D}(w_c)+12\,\beta_4\bar{E}(w_c)+\ldots\right)\quad\text{FCC alloys} \tag{61a}$$

$$\Delta\widetilde{E}^2_{\text{p},sd}(w_c)\approx\left(\mu\cdot\frac{1+\nu}{1-\nu}\right)^2\left(\beta_0\,\bar{A}(w_c)+8\,\beta_1\,\bar{B}(w_c)+6\,\beta_2\,\bar{C}(w_c)+12\,\beta_3\,\bar{D}(w_c)+24\,\beta_4\bar{E}(w_c)+\ldots\right)\quad\text{BCC alloys} \tag{61b}$$

The above results provide *analytic* formulae for the solute-dislocation strengthening in the presence of SRO within the elasticity approximation that involves the solute misfit volumes. These analytic results fully

quantify the interplay in strengthening between solute misfit volumes and SRO in a general multicomponent alloy.

		NN(w_c^A)			NN$'$(w_c^A) b			NN$''$(w_c^A) b^2		
	σ/b	1.5 (fcc)	2.0 (fcc)	1.33 (bcc)	1.5 (fcc)	2.0 (fcc)	1.33 (bcc)	1.5 (fcc)	2.0 (fcc)	1.33 (bcc)
NN	A	0.1008	0.0889	0.337	0.02276	0.017	0.07688	-0.0059	-0.0037	-0.0192
	B	0.07	0.0661	0.2323	0.01835	0.014	0.064	-0.0031	-0.0023	-0.00957
	C	0.0433	0.04534	0.2041	0.01372	0.011	0.0591	-0.00078	-0.001	-0.006857
	D	0.0464	0.04761	0.1493	0.0142	0.0113	0.05056	-0.0011	-0.00116	-0.0018
	E	0.0485	0.04947	0.1345	0.01475	0.0116	0.04615	-0.0013	-0.0013	-0.000567

Table 2: Coefficients A,B,C,D,E and their first and second derivatives evaluated at w_c^A for (a) fcc edge dislocations with partial separation $d_p = 15b$ and partial core spread $\sigma/b = 1.5, 2.0$ and (b) bcc edge dislocations with compact core of width $\sigma = 1.3333b$. $w_c^A = 4.5b, 5.5b$ for $\sigma = 1.5b, 2.0b$ in fcc and $w_c^A = 4.3333b$ for $\sigma = 1.33b$ in bcc.

Figure 4 presents the percent changes in ΔE_b and τ_{y0} relative to the random alloy for fcc edge dislocations with $\sigma = 1.5b$ in multicomponent alloys as function of two normalized SRO parameters β_1/β_0 and $\overline{\beta}/\beta_0 = (\beta_2 + 4\beta_3 + 2\beta_4)/\beta_0$ (recalling $\beta_0 = \sum_n c_n \Delta V_n^2$ and $\beta_i = \sum_{n,m>n} c_n c_m (\Delta V_n - \Delta V_m)^2 \alpha_{nm}$). The latter quantity combines SRO contributions for all neighbors beyond first neighbors and can be used because the coefficients C,D,E are essentially identical (see Figure 3a, Table 2). With this notation, $\Delta\widetilde{E}^2_{\mathrm{p},sd}(w_c)$ takes the following form

$$\Delta\widetilde{E}^2_{\mathrm{p},sd}(w_c) \approx \left(\mu \cdot \frac{1+\nu}{1-\nu}\right)^2 \beta_0 \left[A(w_c) + 12\, B(w_c)\, \frac{\beta_1}{\beta_0} + 6\, C(w_c)\, \frac{\overline{\beta}}{\beta_0}\right] \tag{62}$$

where the random alloy corresponds to $\beta_1 = 0, \overline{\beta} = 0$. Jumps in the curves correspond to the discrete changes in w_c by $b/2$ (Figure 5). Predictions using the (smooth) w_c and $\Delta\widetilde{E}^2_{\mathrm{p},sd}(w_c)$ as calculated from Equations 58a and 62 with approximate coefficients $\bar{A}$, $\bar{B}$ and $\bar{C}$ are shown as dashed lines in Figure 4.

Moderate SRO has a noticeable effect on both the energy barrier ΔE_b and the 0K flow stress $\Delta\tau_{y0}$. For first-neighbor SRO only, the energy barrier and strength can vary by $\pm 25-30\%$ over the range $\beta_1/\beta_0 \pm 0.06$. Similarly, in the absence of first-neighbor SRO, the energy barrier and strength can vary by $\pm 20\%$ and $\pm 10\%$ respectively over the range $\overline{\beta}/\beta_0 \pm 0.10$. Often, however, first and second neighbors can have opposite-sign SRO parameters, leading to some cancellation. For instance, for the combination $\beta_1/\beta_0 = -0.06$, $\overline{\beta}/\beta_0 = +0.10$, the barrier and strength are reduced by only about 10% and 15%, respectively. Similar cancellations arise for $\beta_1/\beta_0 = +0.06$, $\overline{\beta}/\beta_0 = -0.10$. In general, it unlikely that both β_1/β_0 and $\overline{\beta}/\beta_0$ have the same sign, and hence there is likely some tendency for cancellation. The approximate analytic estimates using Equations 58a and 61a are seen to be reasonably accurate, with only notable deviations in $\Delta\tau_{y0}$ for negative values of $\beta_1/\beta_0 < -0.025$ and $\overline{\beta}/\beta_0 = -0.1$. Changes in w_c are shown in Figure 5 and are small but not negligible relative to the random alloy value of $w_c = 4.5b$. Negative values of SRO reduce w_c and, since $\Delta\tau_{y0} \propto w_c^{-5/3}$ and $\Delta E_b \propto w_c^{2/3}$ (Equations 32, 31), increase the zero-T strength but reduced the barrier but we nonetheless find decreases in zero-T strength even with reduced w_c. *Figure 4 serves as a design guideline for all multicomponent fcc alloys with SRO pair correlations extending up to* 4^{th}NN *and is a major practical result of our analysis.*

As an example application, we consider the NiCoCr alloy as studied by Du et al. [46]. They used a machine-learned interatomic potential and calculated the WC-SRO parameters via a hybrid Monte Carlo/molecular dynamics simulation. Using the computed SRO parameters at $T = 1000\ K$, around where SRO is reported to develop experimentally [27], along with the experimentally-derived solute misfit volumes for Ni, Co, and Cr [47], yields $\beta_1/\beta_0 = -0.0557$ and $\bar{\beta}/\beta_0 = 0.1064$. These then correspond to changes in ΔE_b and $\Delta\tau_{y0}$ of -6.63% and -12.82% respectively, as indicated by the star points in Figures 4 and 5 and with $w_c = 4.5b$ unchanged from the random-alloy value. With the random alloy strength and barrier computed by Yin et al. [47] of $\tau_{y0} = 124.5$ MPa and $\Delta E_b = 1.29$ eV, the room-temperature critically-resolved shear stress (CRSS) is predicted to be *reduced* from 64 MPa to 54 MPa. This reduction will be offset by some positive τ_A, but τ_A depends strongly on the interatomic potential, and first-principles calculations in the magnetic Co-Cr-Fe-Mn-Ni Cantor alloy family are challenging [47, 48]. Hence the potentials derived from first

principles are not necessarily quantitatively valid, and we use them here only to obtain some likely-reasonable SRO parameters. With that caveat, our prediction that SRO reduces the dominant solute/dislocation or misfit contribution to strengthening along with the some positive τ_A may rationalize recent experimental results showing that SRO has essentially no effect on CRSS in NiCoCr samples annealed in temperature range of 673 – 973 K [27]. Note that this is an example of the application of the theory and is not a validation of the theory.

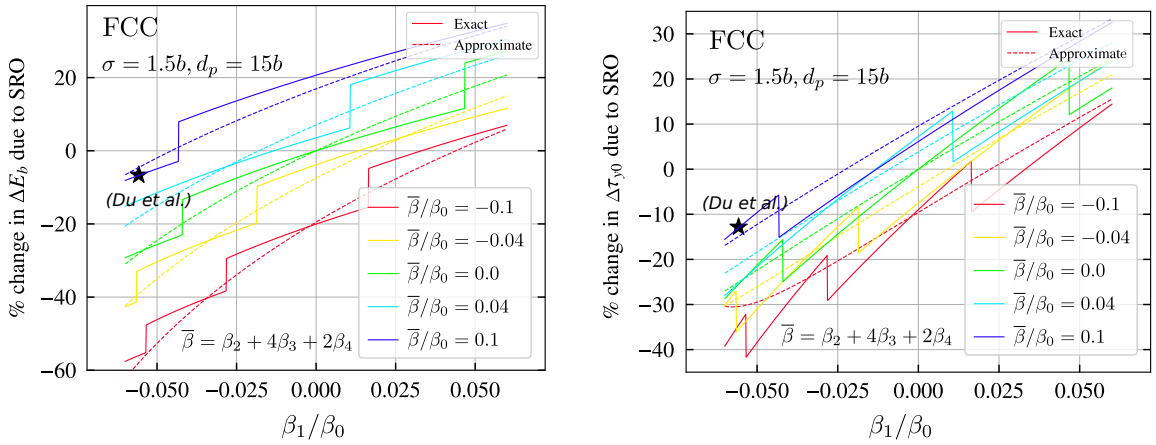

(a) Percent change in the energy barrier

(b) Percent change in T=0K yield strength

Figure 4: Percent change in critical solid solution hardening quantities in fcc alloys relative to the random alloy as function of two SRO parameters β_1/β_0 and $\overline{\beta}/\beta_0 = (\beta_2 + 4\beta_3 + 2\beta_4)/\beta_0$. Dashed lines show approximate estimates using Equations 59 and 62 with values from Table 2. Predictions for NiCoCr using WC-SRO parameters from Ref. [46] and misfit volumes from Ref. [47] are marked with a black star.

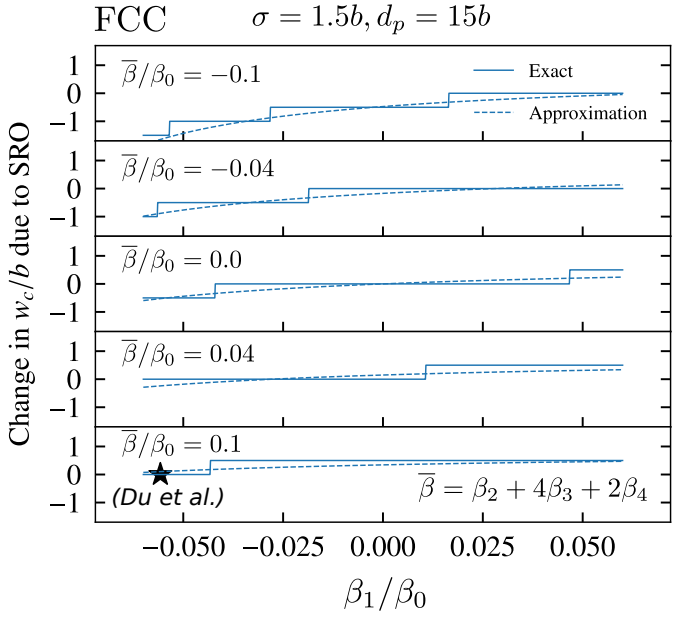

Figure 5: Change in characteristic dislocation roughening amplitude w_c in fcc alloys relative to the random alloy value of $4.5b$, as function of β_1/β_0 and $\overline{\beta}/\beta_0$. Dashed lines are approximate estimates using Equations 59 with values from Table 2.

Equation 54b for bcc alloys, can be expressed along the same lines as Equation 62 above. To reduce the complexity, we note that the bcc coefficients are approximately $B \approx 1.15C$ and $D \approx 1.1E$ for $w/b < 7$, which is within the range of w_c values for moderate SRO. This gives us

$$\Delta\widetilde{E}^2_{\mathrm{p},sd}(w_c) \approx \left(\mu \cdot \frac{1+\nu}{1-\nu}\right)^2 \beta_0 \left[A(w_c) + 6\,C(w_c)\,\frac{\overline{\beta}_1}{\beta_0} + 12\,D(w_c)\,\frac{\overline{\beta}_2}{\beta_0}\right] \tag{63}$$

in terms of two other dimensionless SRO parameters $\overline{\beta}_1 = 1.5\,\beta_1 + \beta_2$ and $\overline{\beta}_2 = \beta_3 + 1.8\,\beta_4$,

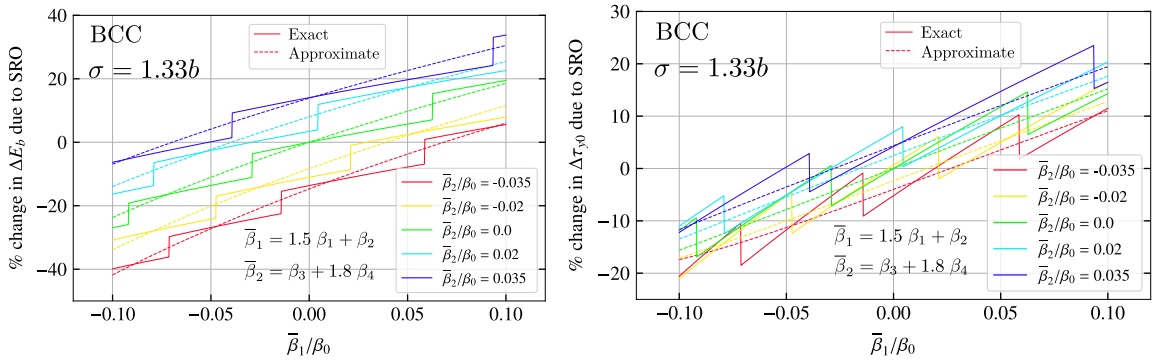

(a) Percent change in the energy barrier

(b) Percent change in T=0K yield strength

Figure 6: Percent change in critical solid solution hardening quantities in bcc alloys relative to a random alloy as function of two SRO parameters $\overline{\beta}_1/\beta_0 = (1.5\,\beta_1 + \beta_2)/\beta_0$ and $\overline{\beta}_2/\beta_0 = (\beta_3 + 1.8\,\beta_4)/\beta_0$. Dashed lines are approximate estimates using Equations 60 and 63 with values from Table 2.

In bcc alloys, moderate SRO has considerable effects of $\pm 20\%$ on the energy barrier ΔE_b and over $\pm 12\%$ on the 0K flow stress τ_{y0} over the range $\overline{\beta}_1/\beta_0 \pm 0.1$. The approximate analytic estimates (Equations 58b and 61b) are reasonably accurate for the energy barrier but show larger deviations for the strength, with jumps in the full results corresponding to changes in the discrete (increments of $b/3$) value of w_c (Figure 7). As for fcc alloys, changes in w_c due to SRO are small but not negligible relative to the random alloy value of $w_c = 4.3333b$ and are reported in Figure 7.

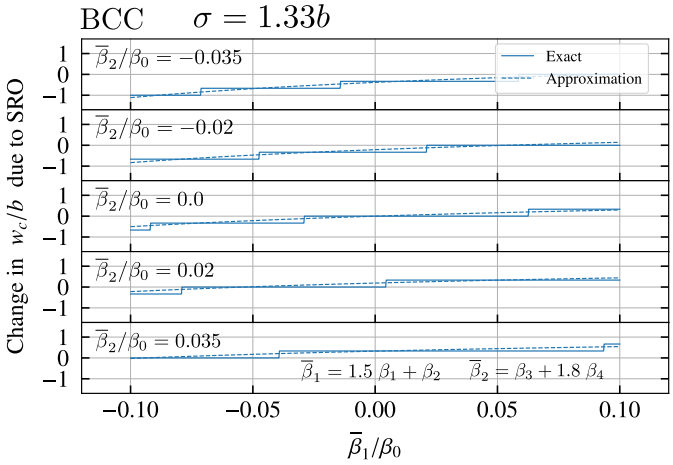

Figure 7: Change in characteristic dislocation roughening amplitude w_c in bcc alloys with respect to the random alloy value of $4.3333b$, as function of combined quantities $\overline{\beta}_1/\beta_0$ and $\overline{\beta}_2/\beta_0$. Dashed lines are for approximate estimates using Equations 60 with values from Table 2.

Forthcoming work by Xin and Curtin [49] will explicitly demonstrate the negative and positive effects of SRO on strength in a model bcc alloy using carefully-designed atomistic simulations. This will constitute quantitative validation of the present theory.

5.2. Strengthening due to solute-solute interactions

In Section 4.1, we have derived a general expression for the athermal strengthening τ_A (Equation 24) due to solute-solute interactions in terms of alloy concentration, EPIs, and WC-SRO parameters, for any fcc or bcc alloy. Although this is the most general expression of τ_A derived to date, atomic interactions in concentrated alloys can be many-body, i.e. extend beyond just pair interactions. In such cases, although a cluster expansion (CE) model or multi-body interatomic potential can be used to capture the solute interactions among atoms in the crystal, we have no analytical expression for τ_A. For the thermally activated strengthening contribution, our derived results for $\sigma^2_{\Delta E_{ss,f}}$ and $\sigma^2_{\Delta E_{ss,p}}$ in Section 4.2.3 are also quite complicated and not easily simplified nor easily generalized to multi-body interactions.

If a CE or interatomic potential or, at much higher cost, first-principles density function theory (DFT) is available, however, strengthening due to solute-solute interactions with and without SRO can be computed.

First, the relevant equilibrium SRO in an alloy is modeled using Monte-Carlo simulations along with the CE/interatomic potential/DFT. Starting from the resulting atomistic realization of the alloy, with or without SRO, the energy change per unit area due to full slip by a Burgers vector can be computed by shifting one-half of the crystal by **b** relative to the other half, across the desired glide plane, and dividing by the slipped area of the sample. Averaging over many realizations with the same SRO, or over a very large area, gives precisely the quantity γ_{SRO} needed to compute the athermal strengthening. In the absence of SRO, the result will be $\gamma_{SRO} = 0$. Furthermore, the statistical distribution of energy changes per unit area measured across the many realizations can be used to compute the fluctuating energy due to solute-solute interactions in the alloy, again with or without SRO. The standard deviation σ_{s-s} of the distribution of energy changes calculated in a simulation cell with N_{slip} atoms on (one side of) the slip plane is converted into the fluctuation energy as $\sigma_{\Delta E_{ss,f}} = \sigma_{s-s}/\sqrt{N_{slip}}$. This approach has recently been used to compute $\sigma_{\Delta E_{ss,f}}$ in the binary AuNi alloy using first-principles density functional theory [40]. Repeating the exact analysis detailed above for partial slip in fcc yields the average stacking fault energy (see Appendix A) and its standard deviation $\sigma_{\Delta E_{ss,p}}$.

We also recall that Ref. [6] showed that the characteristic dislocation waviness amplitude w_c is independent of $\sigma^2_{\Delta E_{ss,p}}$ for $w < d_p$ (partialseparation). This is the situation for many fcc complex concentration alloys with low stacking fault energies and thus with $d_p > 6b$ and then $w_c < d_p$. This result then allows for the computations of w_c and $\Delta\widetilde{E}^2_{\mathrm{p},sd}(w_c)$ as shown in section 5.1 followed by the addition of $\sigma_{\Delta E_{ss,p}}$ according to Equation 38. This feature greatly simplifies the incorporation of the solute-solute fluctuation contribution into the solute-strengthening theory [40].

6. Conclusion

A theory of solute strengthening for random alloys has been extended to incorporate the effects of short-range ordering (SRO) that can exist in alloys. The degree of SRO depends on alloy chemical interactions, solute kinetics, and time-temperature processing conditions and is not addressed here. The theory is developed in the framework of the widely-used Warren-Cowley SRO parameters and in terms of effective pair interactions (EPIs) to describe the solute-solute interactions.

In the presence of SRO, there is an athermal strengthening due to the energy cost in shearing of an SRO structure. This strengthening contribution has been well-recognized in the literature. The present work extends the results to arbitrary multicomponent fcc and bcc alloys within the framework of EPIs.

More interestingly, the atomic correlations implied by any SRO in the alloy affect the fluctuations in the solute-dislocation interaction energy parameter ($\Delta\widetilde{E}^2_{\mathrm{p}}$) that controls strengthening in the random alloy. This change in alloy strength is independent of any energetic description such as EPIs (although the SRO is due to the solute-solute interactions). The full theory has been reduced to simpler forms using the elasticity approximation and solute misfit volumes to estimate the individual solute/dislocation interaction energies that combine to give $\Delta\widetilde{E}^2_{\mathrm{p}}$. This rigorous analysis reveals that this SRO contribution to strengthening can either increase or decrease the alloy strength. The possibility of a decreased strength due to SRO arises primarily when the SRO parameters are negative (attraction of unlike solutes) and the differences in misfit volumes of the unlike pairs are large. The theory predicts changes in the energy barrier and T=0K strength of 10–30% for fcc alloys, either positive or negative, for moderate levels of SRO. For bcc alloys, the energy barriers changes of 10–35% are similar while changes in 0K yield stress are smaller (< 10%). Analytic results are provided to facilitate application of this solute/dislocation strengthening theory in terms of alloy elastic constants, solute misfit volumes, and SRO parameters; no knowledge of solute-solute interactions is required.

Since the strength of many HEAs to date can be reasonably captured by the solute/dislocation interaction contribution, the effects of SRO on strength due to the solute/dislocation contribution may be comparable to, or larger than, those due to the athermal strengthening. If the SRO effects are negative (decreasing strength), then they will offset the positive athermal strengthening. This may lead to a lower net strengthening of the alloy relative to the random alloy and even, possibly, overall reduced strengthening. We have applied the analysis here to a model NiCoCr system and have shown a reduction in misfit strengthening at room temperature of 15%, which may offset the positive τ_A and rationalize recent experiments that show limited, if any, strengthening due to SRO [26, 27].

Another contribution to the strengthening, with or without SRO, arises due to fluctuations in the solute-solute interaction energy parameter. While general analytic results are derived, they are complex and not easily applied. We have suggested various computational approaches to estimate these contributions to the strength changes of the alloy.

The parameter-free strengthening theory presented in this work is, to our knowledge, the only complete theory for multicomponent alloys possessing SRO. Importantly, the theory properly reduces to the random

alloy theory when there is zero SRO, and so provides a continuous picture of alloy strengthening versus SRO. As with any theory, approximations have been made in the derivation, and so the theory is not exact. However, the theory does not introduce any ad-hoc parameters and so is broadly applicable. The theory is limited mainly by the ability to estimate the underlying *material* parameters that enter the theory. The theory can thus be used to interpret/rationalize experimental data, guide alloy design toward systems with SRO characteristics that will improve alloy properties, or help assess whether pursuing the creation/control of SRO would lead to notable improvements in alloy performance.

Acknowledgements This work was supported by the Swiss National Science Foundation through the project "Harnessing atomic-scale randomness: design and optimization of mechanical performance in High Entropy Alloys", project "20 0 021_18198/1" and by the NCCR MARVEL, a National Centre of Competence in Research, funded by the Swiss National Science Foundation (grant number 205602). The authors also thank Dr. J.-P. Du and Prof. S. Ogata for sharing their NiCoCr SRO data.

Appendix

A. Stable stacking fault energy γ_{ssfe} in alloys with SRO

The stable stacking fault energy γ_{ssfe} in an fcc crystal is the excess energy per unit area due to slip by a Shockley partial Burgers vector. This is precisely the quantity $\langle \Delta E_{ss,p+} \rangle / A_s$. Therefore, using Equation 18b, we can simplify $\langle \Delta E_{ss,p+} \rangle$ as

$$\langle \Delta E_{ss,p+} \rangle = -\frac{1}{2} \sum_{p,q} c_p c_q \sum_{\substack{k,l \\ y_k<0 \\ y_l>0}} \lambda_{pq}^{kl} \left(V_{pq}^{eff}(d_{kl}^f) - V_{pq}^{eff}(d_{kl}) \right) + \frac{1}{2} \sum_p c_p \sum_i \Delta\varepsilon_i^p \tag{A.1}$$

The first term in the above equation has the same form as the right-hand side in Equation 21 for $\langle \Delta E_{ss,f} \rangle$. So it will have the form of Equation 22 after factoring out $\mathbf{N}_a$ and expressing the sum over sites j as a sum over discrete pair distances d and d'. However, the pair distances d and d' across the partially-slipped crystal differ from the bulk crystal, and hence $n_{dd'}$ is also different, as given in Table 1. The number of atoms on slip plane $\mathbf{N}_a$ can also be factored out of the second term in Equation A.1 and the sum over i replaced by a sum over distances d_z from the slip plane, which in the case of fcc are positive integer multiples of $1/\sqrt{3}$. Therefore we can express the stacking fault energy as

$$\begin{aligned} \gamma_{ssfe} = \frac{\langle \Delta E_{ss,p+} \rangle}{A_s} = \frac{\rho_L \rho_G}{2} \sum_{p,q} c_p c_q \sum_d V_{pq}^{eff}(d) \left(\sum_{\substack{d' \\ d' \neq d}} \alpha_{pq}(d') n_{d'd} - \alpha_{pq}(d) M_d \right) \\ - \frac{\rho_L \rho_G}{2} \sum_{p,q} c_p c_q \sum_d V_{pq}^{eff}(d) \left(N_d - M_d \right) + \rho_L \rho_G \sum_p c_p \sum_{d_z} \Delta\varepsilon^p(d_z) \end{aligned} \tag{A.2}$$

The last two terms in Equation A.2 corresponds to the stacking fault in the random alloy, so the change in γ_{ssfe} is

$$\left(\Delta\gamma_{ssfe} \right)_{SRO} = \frac{\rho_L \rho_G}{2} \sum_{p,q} c_p c_q \sum_d V_{pq}^{eff}(d) \left(\sum_{\substack{d' \\ d' \neq d}} \alpha_{pq}(d') n_{d'd} - \alpha_{pq}(d) M_d \right) \tag{A.3}$$

The γ_{ssfe} thus has the exact same form as γ_{SRO} (Equation 26) but is different in detail because the sums include non-fcc distances arising in the stacking fault and their corresponding non-fcc EPIs, and hence different values for the $n_{dd'}$ and M_d.

		Pair distances after slip									
	d'/a / d/a	0.707	1.0	1.155	1.225	1.354	1.414	1.581	1.683	1.732	1.7795
Pair distances before slip	0.707	-	1	0	0	0	0	0	0	0	0
	1.0	1	-	0	2	0	0	0	0	0	0
	1.155	0	0	-	0	0	0	0	0	0	0
	1.225	0	2	2	-	4	0	2	0	0	0
	1.354	0	0	0	0	-	0	0	0	0	0
	1.414	0	0	0	0	4	-	0	2	0	0
	1.581	0	0	0	2	4	0	-	4	2	0
	1.683	0	0	0	0	0	0	0	-	0	0
	1.732	0	0	0	0	0	0	2	0	-	3
	1.7795	0	0	0	0	0	0	0	0	0	-

Table 3: Structure factors $n_{dd'}$ for pairs of normalized pair distances (d, d') for $a/6[211]$ partial slip along $(1\bar{1}\bar{1})$ plane in fcc.

B. Derivation of the different coefficients $A, B, C, D, \ldots$ in $\Delta\widetilde{E}^2_{\mathrm{p},sd}$ (Equation 54)

In this section we will be basically simplifying Equation 53 to end up with Equation 54 with the coefficients $A, B, C, D, \ldots$.

$$\Delta\widetilde{E}^2_{\mathrm{p},sd} = \left(\sum_n c_n \Delta V_n^2\right)\left(\sum_{[i]} \Delta p_i^2(w)\right) - \sum_{n,m} c_n c_m \Delta V_n \Delta V_m \sum_{[i]} \sum_{\substack{j \\ j\neq i}} \Delta p_i(w)\Delta p_j(w)\ \alpha_{nm}^{ij}$$

$$= \left(\sum_n c_n \Delta V_n^2\right)\left(\sum_{[i]} \Delta p_i^2(w)\right) - \sum_n c_n^2 \Delta V_n^2 \sum_{[i]} \sum_{\substack{j \\ j\neq i}} \Delta p_i(w)\Delta p_j(w)\ \alpha_{nn}^{ij}$$

$$- \sum_{n,m\neq n} c_n c_m \Delta V_n \Delta V_m \sum_{[i]} \sum_{\substack{j \\ j\neq i}} \Delta p_i(w)\Delta p_j(w)\ \alpha_{nm}^{ij}$$

Using Equation 11,

$$= \left(\sum_n c_n \Delta V_n^2\right)\left(\sum_{[i]} \Delta p_i^2(w)\right) + \sum_n c_n \Delta V_n^2 \sum_{[i]} \sum_{\substack{j \\ j\neq i}} \Delta p_i(w)\Delta p_j(w) \sum_{m\neq n} \alpha_{nm}^{ij} c_m$$

$$- \sum_{n,m\neq n} c_n c_m \Delta V_n \Delta V_m \sum_{[i]} \sum_{\substack{j \\ j\neq i}} \Delta p_i(w)\Delta p_j(w)\ \alpha_{nm}^{ij}$$

$$= \left(\sum_n c_n \Delta V_n^2\right)\left(\sum_{[i]} \Delta p_i^2(w)\right) + \sum_{n,m>n} c_n c_m \Delta V_n^2 \sum_{[i]} \sum_{\substack{j \\ j\neq i}} \Delta p_i(w)\Delta p_j(w)\ \alpha_{nm}^{ij}$$

$$+ \sum_{n,m<n} c_n c_m \Delta V_n^2 \sum_{[i]} \sum_{\substack{j \\ j\neq i}} \Delta p_i(w)\Delta p_j(w)\ \alpha_{nm}^{ij} - \sum_{n,m>n} c_n c_m \Delta V_n \Delta V_m \sum_{[i]} \sum_{\substack{j \\ j\neq i}} \Delta p_i(w)\Delta p_j(w)\ \alpha_{nm}^{ij}$$

$$- \sum_{n,m<n} c_n c_m \Delta V_n \Delta V_m \sum_{[i]} \sum_{\substack{j \\ j\neq i}} \Delta p_i(w)\Delta p_j(w)\ \alpha_{nm}^{ij}$$

Replacing $\sum_{n,m<n}$ with $\sum_{m,n>m}$ (equivalent way of summing lower-triangular elements),

$$= \left(\sum_n c_n \Delta V_n^2\right)\left(\sum_{[i]} \Delta p_i^2(w)\right) + \sum_{n,m>n} c_n c_m \Delta V_n^2 \sum_{[i]} \sum_{\substack{j \\ j\neq i}} \Delta p_i(w)\Delta p_j(w)\ \alpha_{nm}^{ij}$$

$$+ \sum_{m,n>m} c_n c_m \Delta V_n^2 \sum_{[i]} \sum_{\substack{j \\ j\neq i}} \Delta p_i(w)\Delta p_j(w)\ \alpha_{nm}^{ij} - \sum_{n,m>n} c_n c_m \Delta V_n \Delta V_m \sum_{[i]} \sum_{\substack{j \\ j\neq i}} \Delta p_i(w)\Delta p_j(w)\ \alpha_{nm}^{ij}$$

$$- \sum_{m,n>m} c_n c_m \Delta V_n \Delta V_m \sum_{[i]} \sum_{\substack{j \\ j\neq i}} \Delta p_i(w)\Delta p_j(w)\ \alpha_{nm}^{ij}$$

Swapping dummy indices n and m in the third and fifth terms,

$$= \left(\sum_n c_n \Delta V_n^2\right)\left(\sum_{[i]} \Delta p_i^2(w)\right) + \sum_{n,m>n} c_n c_m \Delta V_n^2 \sum_{[i]} \sum_{\substack{j \\ j\neq i}} \Delta p_i(w)\Delta p_j(w)\ \alpha_{nm}^{ij}$$

$$+ \sum_{n,m>n} c_m c_n \Delta V_m^2 \sum_{[i]} \sum_{\substack{j \\ j\neq i}} \Delta p_i(w)\Delta p_j(w)\ \alpha_{mn}^{ij} - \sum_{n,m>n} c_n c_m \Delta V_n \Delta V_m \sum_{[i]} \sum_{\substack{j \\ j\neq i}} \Delta p_i(w)\Delta p_j(w)\ \alpha_{nm}^{ij}$$

$$- \sum_{n,m>n} c_m c_n \Delta V_m \Delta V_n \sum_{[i]} \sum_{\substack{j \\ j\neq i}} \Delta p_i(w)\Delta p_j(w)\ \alpha_{mn}^{ij}$$

Since $\alpha_{mn}^{ij} = \alpha_{nm}^{ij}$

$$= \left(\sum_n c_n \Delta V_n^2\right)\left(\sum_{[i]} \Delta p_i^2(w)\right) + \sum_{n,m>n} c_n c_m \Delta V_n^2 \sum_{[i]} \sum_{\substack{j \\ j\neq i}} \Delta p_i(w)\Delta p_j(w)\ \alpha_{nm}^{ij}$$

$$+ \sum_{n,m>n} c_n c_m \Delta V_m^2 \sum_{[i]} \sum_{\substack{j \\ j\neq i}} \Delta p_i(w)\Delta p_j(w)\ \alpha_{nm}^{ij} - 2\sum_{n,m>n} c_n c_m \Delta V_n \Delta V_m \sum_{[i]} \sum_{\substack{j \\ j\neq i}} \Delta p_i(w)\Delta p_j(w)\ \alpha_{nm}^{ij}$$

Grouping last three terms,

$$= \left(\sum_n c_n \Delta V_n^2\right)\left(\sum_{[i]} \Delta p_i^2(w)\right) + \sum_{n,m>n} c_n c_m \left(\Delta V_n - \Delta V_m\right)^2 \sum_{[i]} \sum_{\substack{j \\ j\neq i}} \Delta p_i(w)\Delta p_j(w)\ \alpha_{nm}^{ij} \tag{A.4}$$

To proceed further, we will introduce the notation $\Delta p_i(w|a,b)$, which is basically writing $\Delta p_j(w)$ for any site j in terms of another site i as follows

$$\Delta p_i(w|a,b) = \Delta p_j(w) = p(x_i+a-w, y_i+b) - p(x_i+a, y_i+b) \quad \text{(A.5)}$$
$$\text{where } (a,b) = (x_j - x_i, y_j - y_i) \text{ for sites } (i,j)$$

Obviously, by the above definition $\Delta p_i(w|0,0) = \Delta p_i(w)$.

Lemma B.1. *Auto-correlation of the pressure differences $\Delta p_i(w|a,b)$ satisfies the following identities for any a and w which are integer multiples of $1/(2\sqrt{2})$ in fcc and $1/(2\sqrt{3})$ in bcc, and for any b which is an integer multiple of $1/\sqrt{3}$ in fcc and $1/\sqrt{2}$ in bcc*[1]*,*

$$\sum_{[i]} \Delta p_i(w|0,0)\ \Delta p_i(w|a,b) = \sum_{[i]} \Delta p_i(w|0,0)\ \Delta p_i(w|-a,-b) = \sum_{[i]} \Delta p_i(w|0,0)\ \Delta p_i(w|-a,b) = \sum_{[i]} \Delta p_i(w|0,0)\ \Delta p_i(w|a,-b) \quad \text{(A.6)}$$

The identities between 1st and 2nd terms and between 3rd and 4th terms follows from the well-known symmetric property of autocorrelation functions where reversing the sense of the correlating vector leaves the autocorrelation function unchanged. The identity between 1st and 3rd terms, on the other hand, follows from the fact that the pressure field $p(x,y)$ is symmetric along the glide direction x, even for elastically anisotropic solids. Proof of Lemma B.1 is provided at the end of this section.

The notation of $\Delta p_i(w|a,b)$ will allow us to reformulate Equation A.4 by replacing summation of explicit neighbour sites j with summations over neighbour distances, which we will be simplifying further using Lemma B.1.

First we recall that α_{nm}^{ij} depends on intersite distance $\|\boldsymbol{r}_{ij}\|$ where $\Delta p_i(w)$ depends on only the x- and y-coordinates. Therefore, it is possible that two sites i and j at the same neighbour distance $\|\boldsymbol{r}_{ij}\|$ might have different $(x_j - x_i, y_j - y_i)$ and vice versa. Table 4 tabulates the $(x_j - x_i, y_j - y_i)$ of sites j in the neighbourhood of any reference site i up to 4 nearest neighbours (NNs) in fcc and bcc and also enlists the corresponding NN shells to which the sites belong.

[1] the distances are in terms of lattice parameter

$(x_j,y_j)-(x_i,y_i)/a_{fcc}$	n$^{\text{th}}$ NN
$(0,0)$	3$^{\text{rd}}$ NN, 3$^{\text{rd}}$ NN
$\left(\frac{1}{2\sqrt{2}},0\right),\left(-\frac{1}{2\sqrt{2}},0\right)$	1$^{\text{st}}$ NN, 1$^{\text{st}}$ NN
$\left(\frac{1}{\sqrt{2}},0\right),\left(-\frac{1}{\sqrt{2}},0\right)$	1$^{\text{st}}$ NN, 4$^{\text{th}}$ NN, 4$^{\text{th}}$ NN
$\left(0,\frac{1}{\sqrt{3}}\right)$	1$^{\text{st}}$ NN, 2$^{\text{nd}}$ NN
$\left(\frac{1}{2\sqrt{2}},\frac{1}{\sqrt{3}}\right),\left(-\frac{1}{2\sqrt{2}},\frac{1}{\sqrt{3}}\right)$	3$^{\text{rd}}$ NN, 1$^{\text{st}}$ NN
$\left(\frac{1}{\sqrt{2}},\frac{1}{\sqrt{3}}\right),\left(-\frac{1}{\sqrt{2}},\frac{1}{\sqrt{3}}\right)$	2$^{\text{nd}}$ NN, 3$^{\text{rd}}$ NN
$\left(0,-\frac{1}{\sqrt{3}}\right)$	2$^{\text{nd}}$ NN, 1$^{\text{st}}$ NN
$\left(\frac{1}{2\sqrt{2}},-\frac{1}{\sqrt{3}}\right),\left(-\frac{1}{2\sqrt{2}},-\frac{1}{\sqrt{3}}\right)$	1$^{\text{st}}$ NN, 3$^{\text{rd}}$ NN
$\left(\frac{1}{\sqrt{2}},-\frac{1}{\sqrt{3}}\right),\left(-\frac{1}{\sqrt{2}},-\frac{1}{\sqrt{3}}\right)$	3$^{\text{rd}}$ NN, 2$^{\text{nd}}$ NN
$\left(\frac{3}{2\sqrt{2}},0\right),\left(-\frac{3}{2\sqrt{2}},0\right)$	3$^{\text{rd}}$ NN, 3$^{\text{rd}}$ NN
$\left(\sqrt{2},0\right),\left(-\sqrt{2},0\right)$	4$^{\text{th}}$ NN
$\left(\frac{3}{2\sqrt{2}},\frac{1}{\sqrt{3}}\right),\left(-\frac{3}{2\sqrt{2}},\frac{1}{\sqrt{3}}\right)$	3$^{\text{rd}}$ NN
$\left(\frac{3}{2\sqrt{2}},-\frac{1}{\sqrt{3}}\right),\left(-\frac{3}{2\sqrt{2}},-\frac{1}{\sqrt{3}}\right)$	3$^{\text{rd}}$ NN
$\left(0,\frac{2}{\sqrt{3}}\right)$	3$^{\text{rd}}$ NN, 4$^{\text{th}}$ NN
$\left(0,-\frac{2}{\sqrt{3}}\right)$	3$^{\text{rd}}$ NN, 4$^{\text{th}}$ NN
$\left(\frac{1}{2\sqrt{2}},\frac{2}{\sqrt{3}}\right),\left(-\frac{1}{2\sqrt{2}},\frac{2}{\sqrt{3}}\right)$	3$^{\text{rd}}$ NN
$\left(\frac{1}{2\sqrt{2}},-\frac{2}{\sqrt{3}}\right),\left(-\frac{1}{2\sqrt{2}},-\frac{2}{\sqrt{3}}\right)$	3$^{\text{rd}}$ NN
$\left(\frac{1}{\sqrt{2}},\frac{2}{\sqrt{3}}\right),\left(-\frac{1}{\sqrt{2}},\frac{2}{\sqrt{3}}\right)$	4$^{\text{th}}$ NN
$\left(\frac{1}{\sqrt{2}},-\frac{2}{\sqrt{3}}\right),\left(-\frac{1}{\sqrt{2}},-\frac{2}{\sqrt{3}}\right)$	4$^{\text{th}}$ NN

(a) fcc

$(x_j,y_j)-(x_i,y_i)/a_{bcc}$	n$^{\text{th}}$ NN
$\left(-\frac{5}{2\sqrt{3}},-\frac{1}{\sqrt{2}}\right),\left(-\frac{5}{2\sqrt{3}},\frac{1}{\sqrt{2}}\right)$	4$^{\text{th}}$ NN
$\left(\frac{5}{2\sqrt{3}},-\frac{1}{\sqrt{2}}\right),\left(\frac{5}{2\sqrt{3}},\frac{1}{\sqrt{2}}\right)$	4$^{\text{th}}$ NN
$\left(-\frac{5}{2\sqrt{3}},0\right),\left(\frac{5}{2\sqrt{3}},0\right)$	4$^{\text{th}}$ NN
$\left(-\frac{2}{\sqrt{3}},-\frac{1}{\sqrt{2}}\right),\left(-\frac{2}{\sqrt{3}},\frac{1}{\sqrt{2}}\right)$	3$^{\text{rd}}$ NN
$\left(\frac{2}{\sqrt{3}},-\frac{1}{\sqrt{2}}\right),\left(\frac{2}{\sqrt{3}},\frac{1}{\sqrt{2}}\right)$	3$^{\text{rd}}$ NN
$\left(-\frac{2}{\sqrt{3}},0\right),\left(\frac{2}{\sqrt{3}},0\right)$	3$^{\text{rd}}$ NN
$\left(-\frac{3}{2\sqrt{3}},-\sqrt{2}\right),\left(-\frac{3}{2\sqrt{3}},\sqrt{2}\right)$	4$^{\text{th}}$ NN
$\left(\frac{3}{2\sqrt{3}},-\sqrt{2}\right),\left(\frac{3}{2\sqrt{3}},\sqrt{2}\right)$	4$^{\text{th}}$ NN
$\left(-\frac{3}{2\sqrt{3}},-\frac{1}{\sqrt{2}}\right),\left(-\frac{3}{2\sqrt{3}},\frac{1}{\sqrt{2}}\right)$	4$^{\text{th}}$ NN, 4$^{\text{th}}$ NN
$\left(\frac{3}{2\sqrt{3}},-\frac{1}{\sqrt{2}}\right),\left(\frac{3}{2\sqrt{3}},\frac{1}{\sqrt{2}}\right)$	4$^{\text{th}}$ NN, 4$^{\text{th}}$ NN
$\left(\frac{3}{2\sqrt{3}},0\right),\left(-\frac{3}{2\sqrt{3}},0\right)$	1$^{\text{st}}$ NN
$\left(-\frac{1}{\sqrt{3}},-\frac{1}{\sqrt{2}}\right),\left(-\frac{1}{\sqrt{3}},\frac{1}{\sqrt{2}}\right)$	2$^{\text{nd}}$ NN
$\left(\frac{1}{\sqrt{3}},-\frac{1}{\sqrt{2}}\right),\left(\frac{1}{\sqrt{3}},\frac{1}{\sqrt{2}}\right)$	2$^{\text{nd}}$ NN
$\left(-\frac{1}{2\sqrt{3}},-\sqrt{2}\right),\left(-\frac{1}{2\sqrt{3}},\sqrt{2}\right)$	4$^{\text{th}}$ NN
$\left(\frac{1}{2\sqrt{3}},-\sqrt{2}\right),\left(\frac{1}{2\sqrt{3}},\sqrt{2}\right)$	4$^{\text{th}}$ NN
$\left(-\frac{1}{2\sqrt{3}},-\frac{1}{\sqrt{2}}\right),\left(-\frac{1}{2\sqrt{3}},\frac{1}{\sqrt{2}}\right)$	1$^{\text{st}}$ NN
$\left(\frac{1}{2\sqrt{3}},-\frac{1}{\sqrt{2}}\right),\left(\frac{1}{2\sqrt{3}},\frac{1}{\sqrt{2}}\right)$	1$^{\text{st}}$ NN
$\left(\frac{1}{2\sqrt{3}},0\right),\left(-\frac{1}{2\sqrt{3}},0\right)$	1$^{\text{st}}$ NN, 4$^{\text{th}}$ NN
$\left(0,\frac{1}{\sqrt{2}}\right),\left(0,-\frac{1}{\sqrt{2}}\right)$	3$^{\text{rd}}$ NN, 3$^{\text{rd}}$ NN
$\left(0,\sqrt{2}\right),\left(0,-\sqrt{2}\right)$	3$^{\text{rd}}$ NN
$\left(\frac{1}{\sqrt{3}},0\right),\left(-\frac{1}{\sqrt{3}},0\right)$	2$^{\text{nd}}$ NN

(b) bcc

Table 4: First column tabulates the (x_j-x_i,y_j-y_i) of sites j in the neighbourhood of any reference site i up to 4 nearest neighbours (NNs) in (a) fcc and (b) bcc. The second column enumerates the NN distances which corresponds to the corresponding (x_j-x_i,y_j-y_i) value enlisted in column 1. For example, the second row in 4a implies there are two 1$^{\text{st}}$ NN sites which have $(x_j-x_i,y_j-y_i)=(1/2\sqrt{2},0)$ and another two 1$^{\text{st}}$ NN sites which have $(x_j-x_i,y_j-y_i)=(-1/2\sqrt{2},0)$. a_{fcc} and a_{bcc} are fcc and bcc lattice parameters respectively.

We will now simplify Equation A.4 for fcc, using values from Table 4a and the notation $\Delta p_i(w|a,b)$ from Equation A.5. Doing so, $\Delta\widetilde{E}^2_{\text{p},sd}$ can be expressed for fcc alloys with SRO extending up to 4$^{\text{th}}$ NN as follows,

$$
\begin{aligned}
\Delta\widetilde{E}^2_{\mathrm{p},sd} = &\left(\sum_n c_n \Delta V_n^2\right)\left(\sum_{[i]} \Delta p_i^2(w)\right) + \sum_{n,m>n} c_n c_m \left(\Delta V_n - \Delta V_m\right)^2 \Bigg[\\
&+ \sum_{[i]} \Delta p_i(w|0,0) \left(2\Delta p_i\left(w\middle|\pm\frac{a_{fcc}}{2\sqrt{2}},0\right) + \Delta p_i\left(w\middle|\pm\frac{a_{fcc}}{\sqrt{2}},0\right) + \Delta p_i\left(w\middle|0,\pm\frac{a_{fcc}}{\sqrt{3}}\right) \right. \\
&\qquad \left. + \Delta p_i\left(w\middle|\pm\frac{a_{fcc}}{2\sqrt{2}},\pm\frac{a_{fcc}}{\sqrt{3}}\right) \right) \alpha_{nm}(1^{\text{st}}\ \text{NN}) \\
&+ \sum_{[i]} \Delta p_i(w|0,0) \left(\Delta p_i\left(w\middle|0,\pm\frac{a_{fcc}}{\sqrt{3}}\right) + \Delta p_i\left(w\middle|\pm\frac{a_{fcc}}{\sqrt{2}},\pm\frac{a_{fcc}}{\sqrt{3}}\right) \right) \alpha_{nm}(2^{\text{nd}}\ \text{NN}) \\
&+ \sum_{[i]} \Delta p_i(w|0,0) \left(2\Delta p_i(w|0,0) + \Delta p_i\left(w\middle|\pm\frac{a_{fcc}}{2\sqrt{2}},\pm\frac{a_{fcc}}{\sqrt{3}}\right) + \Delta p_i\left(w\middle|\pm\frac{a_{fcc}}{\sqrt{2}},\pm\frac{a_{fcc}}{\sqrt{3}}\right) + 2\Delta p_i\left(w\middle|\pm\frac{3a_{fcc}}{2\sqrt{2}},0\right) \right. \\
&\qquad \left. + \Delta p_i\left(w\middle|\pm\frac{3a_{fcc}}{2\sqrt{2}},\pm\frac{a_{fcc}}{\sqrt{3}}\right) + \Delta p_i\left(w\middle|\pm\frac{a_{fcc}}{2\sqrt{2}},\pm\frac{2a_{fcc}}{\sqrt{3}}\right) + \Delta p_i\left(w\middle|0,\pm\frac{2a_{fcc}}{\sqrt{3}}\right) \right) \alpha_{nm}(3^{\text{rd}}\ \text{NN}) \\
&+ \sum_{[i]} \Delta p_i(w|0,0) \left(2\Delta p_i\left(w\middle|\pm\frac{a_{fcc}}{\sqrt{2}},0\right) + \Delta p_i\left(w\middle|\pm\sqrt{2}\,a_{fcc},0\right) + \Delta p_i\left(w\middle|0,\pm\frac{2a_{fcc}}{\sqrt{3}}\right) \right. \\
&\qquad \left. + \Delta p_i\left(w\middle|\pm\frac{a_{fcc}}{\sqrt{2}},\pm\frac{2a_{fcc}}{\sqrt{3}}\right) \right) \alpha_{nm}(4^{\text{th}}\ \text{NN}) \quad \Bigg]
\end{aligned} \tag{A.7}
$$

where we have introduced a new operator $\pm$ to group equivalent auto-correlation terms and is defined as follows,

$$
\begin{aligned}
\Delta p_i(w|\pm a,0) &= \Delta p_i(w|a,0) + \Delta p_i(w|-a,0) \quad \forall a \neq 0 \\
\Delta p_i(w|0,\pm b) &= \Delta p_i(w|0,b) + \Delta p_i(w|0,-b) \quad \forall b \neq 0 \\
\Delta p_i(w|\pm a,\pm b) &= \Delta p_i(w|a,b) + \Delta p_i(w|a,-b) + \Delta p_i(w|-a,b) + \Delta p_i(w|-a,-b) \quad \forall a,b \neq 0
\end{aligned} \tag{A.8}
$$

The operator $\pm$ has the following properties derived from Lemma B.1.

$$
\begin{aligned}
\sum_{[i]} \Delta p_i(w|0,0)\,\Delta p_i(w|\pm a,0) &= 2\sum_{[i]} \Delta p_i(w|0,0)\,\Delta p_i(w|a,0) \quad \forall a \neq 0 \\
\sum_{[i]} \Delta p_i(w|0,0)\,\Delta p_i(w|0,\pm b) &= 2\sum_{[i]} \Delta p_i(w|0,0)\,\Delta p_i(w|0,b) \quad \forall b \neq 0 \\
\sum_{[i]} \Delta p_i(w|0,0)\,\Delta p_i(w|\pm a,\pm b) &= 4\sum_{[i]} \Delta p_i(w|0,0)\,\Delta p_i(w|a,b) \quad \forall a,b \neq 0
\end{aligned} \tag{A.9}
$$

Therefore, number of auto-correlation terms on RHS in Equation A.7 reduces from 33 to 12 and we have

$$\begin{aligned}
\Delta\widetilde{E}^2_{\mathrm{p},sd} = &\left(\sum_n c_n \Delta V_n^2\right)\left(\sum_{[i]} \Delta p_i^2(w)\right) + \sum_{n,m>n} c_n c_m \left(\Delta V_n - \Delta V_m\right)^2 \Bigg[\\
&+2\sum_{[i]} \Delta p_i\left(w|0,0\right) \Bigg(2\Delta p_i\left(w\Big|\frac{a_{fcc}}{2\sqrt{2}},0\right) + \Delta p_i\left(w\Big|\frac{a_{fcc}}{\sqrt{2}},0\right) + \Delta p_i\left(w\Big|0,\frac{a_{fcc}}{\sqrt{3}}\right) \\
&\qquad +2\Delta p_i\left(w\Big|\frac{a_{fcc}}{2\sqrt{2}},\frac{a_{fcc}}{\sqrt{3}}\right)\Bigg)\alpha_{nm}(1^{\text{st}}\text{ NN}) \\
&+2\sum_{[i]} \Delta p_i\left(w|0,0\right) \left(\Delta p_i\left(w\Big|0,\frac{a_{fcc}}{\sqrt{3}}\right) + 2\Delta p_i\left(w\Big|\frac{a_{fcc}}{\sqrt{2}},\frac{a_{fcc}}{\sqrt{3}}\right)\right)\alpha_{nm}(2^{\text{nd}}\text{ NN}) \\
&+2\sum_{[i]} \Delta p_i\left(w|0,0\right) \Bigg(\Delta p_i\left(w|0,0\right) + 2\Delta p_i\left(w\Big|\frac{a_{fcc}}{2\sqrt{2}},\frac{a_{fcc}}{\sqrt{3}}\right) + 2\Delta p_i\left(w\Big|\frac{a_{fcc}}{\sqrt{2}},\frac{a_{fcc}}{\sqrt{3}}\right) + 2\Delta p_i\left(w\Big|\frac{3a_{fcc}}{2\sqrt{2}},0\right) \\
&\qquad +2\Delta p_i\left(w\Big|\frac{3a_{fcc}}{2\sqrt{2}},\frac{a_{fcc}}{\sqrt{3}}\right) + 2\Delta p_i\left(w\Big|\frac{a_{fcc}}{2\sqrt{2}},\frac{2a_{fcc}}{\sqrt{3}}\right) + \Delta p_i\left(w\Big|0,\frac{2a_{fcc}}{\sqrt{3}}\right)\Bigg)\alpha_{nm}(3^{\text{rd}}\text{ NN}) \\
&+2\sum_{[i]} \Delta p_i\left(w|0,0\right) \Bigg(2\Delta p_i\left(w\Big|\frac{a_{fcc}}{\sqrt{2}},0\right) + \Delta p_i\left(w\Big|\sqrt{2}\,a_{fcc},0\right) + \Delta p_i\left(w\Big|0,\frac{2a_{fcc}}{\sqrt{3}}\right) \\
&\qquad +2\Delta p_i\left(w\Big|\frac{a_{fcc}}{\sqrt{2}},\frac{2a_{fcc}}{\sqrt{3}}\right)\Bigg)\alpha_{nm}(4^{\text{th}}\text{ NN}) \Bigg]
\end{aligned} \tag{A.10}$$

The nearest neighbour coordination numbers can be factored out from the coefficients of α_{AB} at the respective pair distances in Equation A.10. In the case of elastically isotropic alloy, the elastic constant dependence of $\Delta p_i(w)$ can also be factored out as $\mu(1+\nu)/(1-\nu)$ and the resultant coefficients of α_{AB} at different pair distances are then renamed with alphabets $A, B, C, D, E, \ldots$ as in Equation 54, each of which only depends on the dislocation roughening amplitude w *(The colors in Equation A.10 follows the same convention used to designate the different coefficients of α_{AB} in Figure 3).*

Now, simplifying Equation A.4 for bcc, using values from Table 4b and Equation A.9, we have $\Delta\widetilde{E}^2_{\mathrm{p},sd}$ for bcc alloys with SRO extending up to 4$^{\text{th}}$ NN as follows

$$\begin{aligned}
\Delta\widetilde{E}^2_{\mathrm{p},sd} = &\left(\sum_n c_n \Delta V_n^2\right)\left(\sum_{[i]} \Delta p_i^2(w)\right) + \sum_{n,m>n} c_n c_m \left(\Delta V_n - \Delta V_m\right)^2 \Bigg[\\
&+2\sum_{[i]} \Delta p_i\left(w|0,0\right) \left(\Delta p_i\left(w\Big|\frac{3a_{bcc}}{2\sqrt{3}},0\right) + \Delta p_i\left(w\Big|\frac{a_{bcc}}{2\sqrt{3}},0\right) + 2\,\Delta p_i\left(w\Big|\frac{a_{bcc}}{2\sqrt{3}},\frac{a_{bcc}}{\sqrt{2}}\right)\right)\alpha_{nm}(1^{\text{st}}\text{ NN}) \\
&+2\sum_{[i]} \Delta p_i\left(w|0,0\right) \left(2\,\Delta p_i\left(w\Big|\frac{a_{bcc}}{\sqrt{3}},\frac{a_{bcc}}{\sqrt{2}}\right) + \Delta p_i\left(w\Big|\frac{a_{bcc}}{\sqrt{3}},0\right)\right)\alpha_{nm}(2^{\text{nd}}\text{ NN}) \\
&+2\sum_{[i]} \Delta p_i\left(w|0,0\right) \Bigg(2\,\Delta p_i\left(w\Big|\frac{2a_{bcc}}{\sqrt{3}},\frac{a_{bcc}}{\sqrt{2}}\right) + \Delta p_i\left(w\Big|\frac{2a_{bcc}}{\sqrt{3}},0\right) + 2\,\Delta p_i\left(w\Big|0,\frac{a_{bcc}}{\sqrt{2}}\right) \\
&\qquad +\Delta p_i\left(w\Big|0,\sqrt{2}a_{bcc}\right)\Bigg)\alpha_{nm}(3^{\text{rd}}\text{ NN}) \\
&+2\sum_{[i]} \Delta p_i\left(w|0,0\right) \Bigg(2\,\Delta p_i\left(w\Big|\frac{5a_{bcc}}{2\sqrt{3}},\frac{a_{bcc}}{\sqrt{2}}\right) + \Delta p_i\left(w\Big|\frac{5a_{bcc}}{2\sqrt{3}},0\right) + 2\,\Delta p_i\left(w\Big|\frac{3a_{bcc}}{2\sqrt{3}},\sqrt{2}a_{bcc}\right) \\
&\qquad +4\,\Delta p_i\left(w\Big|\frac{3a_{bcc}}{2\sqrt{3}},\frac{a_{bcc}}{\sqrt{2}}\right) + 2\,\Delta p_i\left(w\Big|\frac{a_{bcc}}{2\sqrt{3}},\sqrt{2}a_{bcc}\right) + \Delta p_i\left(w\Big|\frac{a_{bcc}}{2\sqrt{3}},0\right)\Bigg)\alpha_{nm}(4^{\text{th}}\text{ NN})\Bigg]
\end{aligned} \tag{A.11}$$

For the plots in Figure 3, the pressure field $p(x_i, y_i)$ is calculated using superposition of isotropic elastic

Volterra solution of pressure due to a discretized smeared out dislocation core, parameterized by double-Gaussian function for fcc [3, 42] and a unimodal Gaussian function for bcc.

For the special case of a binary alloy with concentrations c and $(1-c)$ and misfit volumes ΔV and $-c\Delta V/(1-c)$ respectively, the Equation A.10 simplified to 55. The composition/misfit-volume dependent factor with $A(w)$ simplifies to $\frac{c}{(1-c)}\Delta V^2$ as follows,

$$\sum_n c_n \Delta V_n^2 = c\Delta V^2 + \frac{c^2}{1-c}\Delta V^2 = \frac{c}{(1-c)}\Delta V^2 \tag{A.12}$$

The composition/misfit-volume/correlation dependent factor with $B(w), C(w), \ldots$ also simplifies to $\frac{c}{(1-c)}\Delta V^2 \alpha(\text{n}^{\text{th}}\text{NN})$ as follows

$$\begin{aligned}\sum_{n,m>n} c_n c_m \left(\Delta V_n - \Delta V_m\right)^2 \alpha_{nm}(\text{n}^{\text{th}}\text{NN}) &= c(1-c)\left(\Delta V + \frac{c}{1-c}\Delta V\right)^2 \alpha(\text{n}^{\text{th}}\text{NN}) \\ &= \frac{c}{1-c}\Delta V^2\ \alpha(\text{n}^{\text{th}}\text{NN})\end{aligned} \tag{A.13}$$

So in the binary case, the concentration/misfit-volume dependence can be decoupled from the pair correlations, however this is not possible for the multicomponent alloys. Nevertheless, the neighbour-dependent coefficients $A, B, C, \ldots$ remains the same and Equation 54 can be exactly evaluated with the knowledge of alloy composition, misfit volumes and the Warren-Cowley SRO parameters.

Proof of Lemma B.1. Expanding the auto-correlation function $\sum_{[i]} \Delta p_i(w|0,0)\ \Delta p_i(w|a,b)$ as follows,

$$\begin{aligned}\sum_{[i]} \Delta p_i(w|0,0)\ \Delta p_i(w|a,b) &= \sum_{[i]} \Big(p(x_i - w, y_i) - p(x_i, y_i)\Big)\Big(p(x_i + a - w, y_i + b) - p(x_i + a, y_i + b)\Big) \\ &= \sum_{[i]} p(x_i, y_i)p(x_i + a, y_i + b) - \sum_{[i]} p(x_i, y_i)p(x_i + a - w, y_i + b) \\ &\quad - \sum_{[i]} p(x_i - w, y_i)p(x_i + a, y_i + b) + \sum_{[i]} p(x_i - w, y_i)p(x_i + a - w, y_i + b)\end{aligned} \tag{A.14}$$

one can easily verify that the first and last sums in the RHS are the same by replacing $x_i - w$ with x_i in the last term; basically using the property that auto-correlation is invariant to translation. Therefore we have

$$\begin{aligned}\sum_{[i]} \Delta p_i(w|0,0)\ \Delta p_i(w|a,b) &= 2\sum_{[i]} p(x_i, y_i)p(x_i + a, y_i + b) - \sum_{[i]} p(x_i, y_i)p(x_i + a - w, y_i + b) \\ &\quad - \sum_{[i]} p(x_i - w, y_i)p(x_i + a, y_i + b)\end{aligned} \tag{A.15}$$

To show $\sum_{[i]} \Delta p_i(w|0,0)\ \Delta p_i(w|a,b) = \sum_{[i]} \Delta p_i(w|0,0)\ \Delta p_i(w|-a,-b)$, we replace x_i with $x_i - a$ and y_i with $y_i - b$ in all three auto-correlation terms in the RHS of Equation A.15 and thereby obtain

$$\begin{aligned}\sum_{[i]} \Delta p_i(w|0,0)\ \Delta p_i(w|a,b) &= 2\sum_{[i]} p(x_i - a, y_i - b)p(x_i, y_i) - \sum_{[i]} p(x_i - a, y_i - b)p(x_i - w, y_i) \\ &\quad - \sum_{[i]} p(x_i - a - w, y_i - b)p(x_i, y_i) \\ &= \sum_{[i]} \Delta p_i(w|0,0)\ \Delta p_i(w|-a,-b) \quad \textit{Hence proved.}\end{aligned} \tag{A.16}$$

Identity $\sum_{[i]} \Delta p_i(w|0,0)\ \Delta p_i(w|-a,b) = \sum_{[i]} \Delta p_i(w|0,0)\ \Delta p_i(w|a,-b)$ follows naturally from Equation A.16 for $(-a,b)$ in place of (a,b).

To show $\sum_{[i]} \Delta p_i(w|0,0)\ \Delta p_i(w|a,b) = \sum_{[i]} \Delta p_i(w|0,0)\ \Delta p_i(w|-a,b)$ we will use the symmetry property of edge dislocation pressure field along the glide direction, that is, $p(x_i, y_i) = p(-x_i, y_i)$, in Equation A.15

and obtain

$$\sum_{[i]} \Delta p_i(w|0,0)\ \Delta p_i(w|a,b) = 2\sum_{[i]} p(-x_i,y_i)p(-x_i-a,y_i+b) - \sum_{[i]} p(-x_i,y_i)p(-x_i-a+w,y_i+b)$$
$$-\sum_{[i]} p(-x_i+w,y_i)p(-x_i-a,y_i+b)$$

Since all sites from $-\infty$ to $+\infty$ are summed over, one can replace $-x_i$ with x_i

$$= 2\sum_{[i]} p(x_i,y_i)p(x_i-a,y_i+b) - \sum_{[i]} p(x_i,y_i)p(x_i-a+w,y_i+b)$$
$$-\sum_{[i]} p(x_i+w,y_i)p(x_i-a,y_i+b)$$

Replacing x_i with $x_i - w$ in the last two auto-correlation terms

$$= 2\sum_{[i]} p(x_i,y_i)p(x_i-a,y_i+b) - \sum_{[i]} p(x_i-w,y_i)p(x_i-a,y_i+b)$$
$$-\sum_{[i]} p(x_i,y_i)p(x_i-a-w,y_i+b)$$
$$= \sum_{[i]} \Delta p_i(w|0,0)\ \Delta p_i(w|-a,b) \quad \textit{Hence proved.} \tag{A.17}$$

Note the above derivation could have also been carried out using the anti-symmetric property of edge dislocation pressure field along the slip plane normal, that is, $p(x_i,y_i) = -p(x_i,-y_i)$.

A few caveats to note in the proof of Lemma B.1:

1. Since we have an atomistic system with atoms arranged on fcc or bcc lattice, the pressure field is defined only at the lattice sites (we are ignoring in our analysis the dislocation displacement field). Therefore, keeping in mind the discreteness of our problem, we have the caveat in Lemma B.1 that a and w must be integer multiples of $1/(2\sqrt{2})$ in fcc and $1/(2\sqrt{3})$ in bcc, and b must an integer multiple of $1/\sqrt{3}$ in fcc and $1/\sqrt{2}$ in bcc.
2. The use of the symmetric property of the pressure field in the proof of Equation A.17 requires the mean dislocation position to be at the origin in between two $\{110\}$ planes in fcc or between two $\{111\}$ planes in bcc, considering the discreteness of the lattice. If the dislocation is off the origin in the glide direction by $\pm 1/(4\sqrt{2})$ in fcc or $\pm 1/(4\sqrt{3})$ in bcc, then strictly speaking the symmetry is not satisfied; however the associated error is negligible and exact dislocation position is not well-defined anyway.

C. Covariances $\mathrm{cov}(\Delta E_{sd}, \Delta E_{ss,f})$ in Equation 38

This section justifies why the covariance $\mathrm{cov}(\Delta E_{sd}, \Delta E_{ss,f})$ is negligible compared to the variances $\sigma^2_{\Delta E_{sd}}$ and $\sigma^2_{\Delta E_{ss,f}}$.

First we would simplify $\mathrm{cov}\left(\Delta E_{sd}, \Delta E_{ss,f}\right)$ as follows

$$\mathrm{cov}\left(\Delta E_{sd}, \Delta E_{ss,f}\right) = \langle \Delta E_{sd}\, \Delta E_{ss,f}\rangle - \langle \Delta E_{sd}\rangle \langle \Delta E_{ss,f}\rangle$$
$$\text{Since } \langle \Delta E_{sd}\rangle = 0, \quad \mathrm{cov}\left(\Delta E_{sd}, \Delta E_{ss,f}\right) = \langle \Delta E_{sd}\, \Delta E_{ss,f}\rangle \tag{A.18}$$

Combining Equations 17 and 18a with Equation A.18, we get

$$\mathrm{cov}\left(\Delta E_{sd},\Delta E_{ss,f}\right) = -\frac{1}{2}\left\langle \sum_i \sum_n s_i^n \underbrace{\left(U_{sd}^n(x_i-w,y_i)-U_{sd}^n(x_i,y_i)\right)}_{\Delta U_{sd,i}^n(w)} \sum_{k,l}\sum_{p,q} s_k^p s_l^q \left(V_{pq}^{eff}(d_{kl}^f)-V_{pq}^{eff}(d_{kl})\right)\right\rangle$$

with k,k' being discrete sites below the glide plane and l,l' discrete sites above the glide plane,

$$\begin{aligned}
&= -\frac{1}{2}\sum_{k,l}\sum_{p,q}\left\langle \left(s_k^p\right)^2 s_l^q \right\rangle \Delta U_{sd,k}^p(w)\left(V_{pq}^{eff}(d_{kl}^f)-V_{pq}^{eff}(d_{kl})\right)\\
&-\frac{1}{2}\sum_{k,l}\sum_{p,q}\left\langle s_k^p \left(s_l^q\right)^2 \right\rangle \Delta U_{sd,l}^q(w)\left(V_{pq}^{eff}(d_{kl}^f)-V_{pq}^{eff}(d_{kl})\right)\\
&-\frac{1}{2}\sum_{k',k,l}\sum_{p',p,q}\left\langle s_{k'}^{p'} s_k^p s_l^q \right\rangle \Delta U_{sd,k'}^{p'}(w)\left(V_{pq}^{eff}(d_{kl}^f)-V_{pq}^{eff}(d_{kl})\right)\\
&-\frac{1}{2}\sum_{k,l,l'}\sum_{p,q,q'}\left\langle s_k^p s_l^q s_{l'}^{q'} \right\rangle \Delta U_{sd,l'}^{q'}(w)\left(V_{pq}^{eff}(d_{kl}^f)-V_{pq}^{eff}(d_{kl})\right)\Bigg\rangle\\
&\text{since}\quad \left\langle \left(s_k^p\right)^2 s_l^q \right\rangle = \left\langle s_k^p s_l^q \right\rangle\\
&= -\frac{1}{2}\sum_{k,l}\sum_{p,q}\left\langle s_k^p s_l^q \right\rangle \Delta U_{sd,k}^p(w)\left(V_{pq}^{eff}(d_{kl}^f)-V_{pq}^{eff}(d_{kl})\right)\\
&-\frac{1}{2}\sum_{k,l}\sum_{p,q}\left\langle s_k^p s_l^q \right\rangle \Delta U_{sd,l}^q(w)\left(V_{pq}^{eff}(d_{kl}^f)-V_{pq}^{eff}(d_{kl})\right)\\
&-\frac{1}{2}\sum_{k',k,l}\sum_{p',p,q}\left\langle s_{k'}^{p'} s_k^p s_l^q \right\rangle \Delta U_{sd,k'}^{p'}(w)\left(V_{pq}^{eff}(d_{kl}^f)-V_{pq}^{eff}(d_{kl})\right)\\
&-\frac{1}{2}\sum_{k,l,l'}\sum_{p,q,q'}\left\langle s_k^p s_l^q s_{l'}^{q'} \right\rangle \Delta U_{sd,l'}^{q'}(w)\left(V_{pq}^{eff}(d_{kl}^f)-V_{pq}^{eff}(d_{kl})\right)\Bigg\rangle
\end{aligned} \tag{A.19}$$

Since $U_{sd}^n(x,y) = U_{sd}^n(x,-y)$ due to anti-symmetry of pressure field across the glide plane, $\mathrm{cov}\left(\Delta E_{sd},\Delta E_{ss,f}\right)$ will be zero if atomic positions satisfy reflection symmetry across the glide plane. And the above conclusion holds for any homogeneous alloy, irrespective of the level of SRO. This also implies that $\mathrm{cov}\left(\Delta E_{sd},\Delta E_{ss,f}\right) = 0$ if the stacking sequence of atomic planes along glide plane normal is of $-AAAA-$ type, which is neither the case for fcc nor bcc. Referring to the Figure 2(a) in the middle of the green patch near $w/2$, where the crystallites on either sides of the glide plane are almost fully slipped, the stacking of planes along glide plane normal is close to bulk stacking — therefore, $\mathrm{cov}\left(\Delta E_{sd},\Delta E_{ss,f}\right) \neq 0$. However away from the dislocation core, the dislocation pressure field is negligible near the glide plane making the product $\Delta E_{sd}\cdot\Delta E_{ss,f}$ negligible, and so is the covariance.

On the other hand near the dislocation core, solute-dislocation interaction is the highest. However for edge dislocations due to missing half planes, atomic planes on either sides of the glide plane readjust their position along the glide direction such that reflection symmetry across the glide plane is partially realized near the dislocation core. This in turn reduces $\mathrm{cov}\left(\Delta E_{sd},\Delta E_{ss,f}\right)$ in line with the premise we stated above.

Therefore, overall we think the *covariance* $\mathrm{cov}(\Delta E_{sd},\Delta E_{ss,f})$ *is negligible compared to the variances* $\sigma^2_{\Delta E_{sd}}$ *and* $\sigma^2_{\Delta E_{ss,f}}$*, irrespective of the level of SRO in a homogeneous alloy.*

References

[1] Gerard Paul M Leyson, William A Curtin, Louis G Hector, and Christopher F Woodward. Quantitative prediction of solute strengthening in aluminium alloys. *Nature materials*, 9(9):750–755, 2010.

[2] Gerard Paul M Leyson, LG Hector Jr, and William A Curtin. Solute strengthening from first principles and application to aluminum alloys. *Acta Materialia*, 60(9):3873–3884, 2012.

[3] Céline Varvenne, Aitor Luque, and William A Curtin. Theory of strengthening in fcc high entropy alloys. *Acta Materialia*, 118:164–176, 2016.

[4] Céline Varvenne, Gerard Paul M Leyson, Maryam Ghazisaeidi, and William A Curtin. Solute strengthening in random alloys. *Acta Materialia*, 124:660–683, 2017.

[5] Francesco Maresca and William A Curtin. Mechanistic origin of high strength in refractory bcc high entropy alloys up to 1900K. *Acta Materialia*, 182:235–249, 2020.

[6] S Nag and WA Curtin. Effect of solute-solute interactions on strengthening of random alloys from dilute to high entropy alloys. *Acta Materialia*, 200:659–673, 2020.

[7] N Norman and BE Warren. X-ray measurement of short range order in Ag-Au. *Journal of Applied Physics*, 22(4):483–486, 1951.

[8] P Cenedese, F Bley, and S Lefebvre. Diffuse scattering in disordered ternary alloys: neutron measurements of local order in a stainless steel $Fe_{0.56}Cr_{0.21}Ni_{0.23}$. *Acta Crystallographica Section A: Foundations of Crystallography*, 40(3):228–240, 1984.

[9] JC Fisher. On the strength of solid solution alloys. *Acta metallurgica*, 2(1):9–10, 1954.

[10] PA Flinn. Solute hardening of close-packed solid solutions. *Acta metallurgica*, 6(10):631–635, 1958.

[11] T Mohri, D De Fontaine, and JM Sanchez. Short range order hardening with second neighbor interactions in fcc solid solutions. *Metallurgical Transactions A*, 17(2):189–194, 1986.

[12] LR Owen, HY Playford, HJ Stone, and MG Tucker. Analysis of short-range order in cu3au using x-ray pair distribution functions. *Acta Materialia*, 125:15–26, 2017.

[13] LR Owen, HY Playford, HJ Stone, and MG Tucker. A new approach to the analysis of short-range order in alloys using total scattering. *Acta Materialia*, 115:155–166, 2016.

[14] T Neeraj and MJ Mills. Short-range order (sro) and its effect on the primary creep behavior of a Ti–6wt.% Al alloy. *Materials Science and Engineering: A*, 319:415–419, 2001.

[15] Ruopeng Zhang, Shiteng Zhao, Colin Ophus, Yu Deng, Shraddha J Vachhani, Burak Ozdol, Rachel Traylor, Karen C Bustillo, JW Morris, Daryl C Chrzan, et al. Direct imaging of short-range order and its impact on deformation in Ti-6Al. *Science advances*, 5(12):eaax2799, 2019.

[16] YJ Zhang, D Han, and Xiao Wu Li. A unique two-stage strength-ductility match in low solid-solution hardening Ni-Cr alloys: decisive role of short range ordering. *Scripta Materialia*, 178:269–273, 2020.

[17] D Han, ZY Wang, Y Yan, F Shi, and XW Li. A good strength-ductility match in Cu-Mn alloys with high stacking fault energies: Determinant effect of short range ordering. *Scripta Materialia*, 133:59–64, 2017.

[18] Jun Ding, Qin Yu, Mark Asta, and Robert O Ritchie. Tunable stacking fault energies by tailoring local chemical order in CrCoNi medium-entropy alloys. *Proceedings of the National Academy of Sciences*, 115(36):8919–8924, 2018.

[19] FX Zhang, Shijun Zhao, Ke Jin, H Xue, G Velisa, H Bei, R Huang, JYP Ko, DC Pagan, JC Neuefeind, et al. Local structure and short-range order in a NiCoCr solid solution alloy. *Physical review letters*, 118(20):205501, 2017.

[20] Qing-Jie Li, Howard Sheng, and Evan Ma. Strengthening in multi-principal element alloys with local-chemical-order roughened dislocation pathways. *Nature communications*, 10(1):1–11, 2019.

[21] Soumyadipta Maiti and Walter Steurer. Structural-disorder and its effect on mechanical properties in single-phase TaNbHfZr high-entropy alloy. *Acta Materialia*, 106:87–97, 2016.

[22] Wenqiang Feng, Yang Qi, and Shaoqing Wang. Effects of short-range order on the magnetic and mechanical properties of $FeCoNi(AlSi)_x$ high entropy alloys. *Metals*, 7(11):482, 2017.

[23] E Antillon, C Woodward, SI Rao, B Akdim, and TA Parthasarathy. Chemical short range order strengthening in a model fcc high entropy alloy. *Acta Materialia*, 2020.

[24] Wu-Rong Jian, Zhuocheng Xie, Shuozhi Xu, Yanqing Su, Xiaohu Yao, and Irene J Beyerlein. Effects of lattice distortion and chemical short-range order on the mechanisms of deformation in medium entropy alloy CoCrNi. *Acta Materialia*, 2020.

[25] Andrea Fantin, Giovanni Orazio Lepore, Anna M Manzoni, Sergey Kasatikov, Tobias Scherb, Thomas Huthwelker, Francesco d'Acapito, and Gerhard Schumacher. Short-range chemical order and local lattice distortion in a compositionally complex alloy. *Acta Materialia*, 2020.

[26] Ruopeng Zhang, Shiteng Zhao, Jun Ding, Yan Chong, Tao Jia, Colin Ophus, Mark Asta, Robert O Ritchie, and Andrew M Minor. Short-range order and its impact on the CrCoNi medium-entropy alloy. *Nature*, 581(7808):283–287, 2020.

[27] Le Li, Zhenghao Chen, Shogo Kuroiwa, Mitsuhiro Ito, Koretaka Yuge, Kyosuke Kishida, Hisanori Tanimoto, Yue Yu, Haruyuki Inui, and Easo P George. Evolution of short-range order and its effects on the plastic deformation behavior of single crystals of the equiatomic Cr-Co-Ni medium-entropy alloy. *Acta Materialia*, 243:118537, 2023.

[28] JM Cowley. An approximate theory of order in alloys. *Physical Review*, 77(5):669, 1950.

[29] JM Cowley. Short-range order and long-range order parameters. *Physical Review*, 138(5A):A1384, 1965.

[30] Sheldon Ross. *A first course in probability*. Pearson, 2014.

[31] Y Rao and WA Curtin. Analytical models of short-range order in fcc and bcc alloys. *Acta Materialia*, page 117621, 2022.

[32] JM Sanchez. Cluster expansions and the configurational energy of alloys. *Physical review B*, 48(18):14013, 1993.

[33] JM Sanchez. The cluster expansion method. In *Theory and Applications of the Cluster Variation and Path Probability Methods*, pages 175–185. Springer, 1996.

[34] Juan M Sanchez, Francois Ducastelle, and Denis Gratias. Generalized cluster description of multicomponent systems. *Physica A: Statistical Mechanics and its Applications*, 128(1-2):334–350, 1984.

[35] Anton Van der Ven, John C Thomas, Brian Puchala, and Anirudh Raju Natarajan. First-principles statistical mechanics of multicomponent crystals. *Annual Review of Materials Research*, 48:27–55, 2018.

[36] B Puchala and A Van der Ven. Thermodynamics of the Zr-O system from first-principles calculations. *Physical review B*, 88(9):094108, 2013.

[37] Fritz Körmann, Andrei V. Ruban, and Marcel H.F. Sluiter. Long-ranged interactions in bcc NbMoTaW high-entropy alloys. *Materials Research Letters*, 5(1):35–40, 2017.

[38] GPM Leyson and WA Curtin. Solute strengthening at high temperatures. *Modelling and Simulation in Materials Science and Engineering*, 24(6):065005, 2016.

[39] JH Harris, WA Curtin, and L Schultz. Hydrogen storage characteristics of mechanically alloyed amorphous metals. *Journal of Materials Research*, 3(5):872–883, 1988.

[40] Binglun Yin, Linhan Li, Sophie Drescher, Sascha Seils, Shankha Nag, Jens Freudenberger, and W. A. Curtin. Solute misfit and solute interaction effects on strengthening: a case study in AuNi. *Submitted*, 2023.

[41] Céline Varvenne, Aitor Luque, Wolfram G. Nöhring, and William A. Curtin. Average-atom interatomic potential for random alloys. *Phys. Rev. B*, 93:104201, Mar 2016.

[42] Shankha Nag, Céline Varvenne, and William A Curtin. Solute-strengthening in elastically anisotropic fcc alloys. *Modelling and Simulation in Materials Science and Engineering*, 28(2):025007, 2020.

[43] Céline Varvenne and William A Curtin. Predicting yield strengths of noble metal high entropy alloys. *Scripta Materialia*, 142:92–95, 2018.

[44] Christopher D Woodgate and Julie B Staunton. Short-range order and compositional phase stability in refractory high-entropy alloys via first-principles theory and atomistic modeling: NbMoTa, NbMoTaW, and VNbMoTaW. *Physical Review Materials*, 7(1):013801, 2023.

[45] A Tehranchi, B Yin, and WA Curtin. Solute strengthening of basal slip in mg alloys. *Acta Materialia*, 151:56–66, 2018.

[46] Jun-Ping Du, Peijun Yu, Shuhei Shinzato, Fan-Shun Meng, Yuji Sato, Yangen Li, Yiwen Fan, and Shigenobu Ogata. Chemical domain structure and its formation kinetics in CrCoNi medium-entropy alloy. *Acta Materialia*, 240:118314, 2022.

[47] Binglun Yin, Shuhei Yoshida, Nobuhiro Tsuji, and WA Curtin. Yield strength and misfit volumes of NiCoCr and implications for short-range-order. *Nature communications*, 11(1):2507, 2020.

[48] Christopher D Woodgate, Daniel Hedlund, LH Lewis, and Julie B Staunton. Interplay between magnetism and short-range order in medium-and high-entropy alloys: CrCoNi, CrFeCoNi, and CrMnFeCoNi. *Physical Review Materials*, 7(5):053801, 2023.

[49] X Liu and W. A. Curtin. in preparation.